KYAMBOGO UNIVERSITY

GRADUATE SCHOOL

DEPARTMENT OF MECHANICAL AND MANUFACTURING ENGINEERING

MASTERS THESIS

UTILIZATION OF TOP ALUMINIUM-ZINC DROSS IN THE MANUFACTURE OF PERVIOUS CONCRETE

BY

BATIA STEPHEN

A Master's Thesis submitted to the Graduate School in Partial Fulfillment of the Requirements for the Award of the Master of Science Degree in Advanced Manufacturing Systems Engineering of Kyambogo University

NOVEMBER 2018

KYAMBOGO UNIVERSITY

DEPARTMENT OF MECHANICAL AND MANUFACTURING ENGINEERING

UTILIZATION OF ALUMINIUM-ZINC DROSS IN THE MANUFACTURE OF PERVIOUS CONCRETE

BY

BATIA STEPHEN

(16/U/13438/GMEM/PE)

SUPERVISORS

DR. CATHERINE WANDERA

DR. JEROME .B. SSENGONZI

NOVEMBER 2018

ABSTRACT

Dross is a waste product from the galvanizing process that contains useful substances in large percentages that can be harvested and transformed or reused in production processes to earn a profit. Dross from Roofings Rolling Mills Ltd galvanization process is harvested from the galvanizing bath, cast into blocks and sold to companies that have the technology to extract and process the valuable elements they contain. Though dross from Roofings Rolling Mills Ltd is sold off to other industries that need it, the economic value generated from its sale is not commensurate to the number of valuable products trapped in it. The enormous number of useful products in dross can be utilized in the development of previous concrete slabs to be used in water seepage applications.

Top Al-Zn dross from Roofings Rolling Mills Ltd was analyzed to determine its physical and chemical properties. Top Al-Zn dross was beaten when hot at temperatures below its melting point with a sledgehammer to reduce its size, sorted into three different sizes and mixed to come up with top Al-Zn dross samples. Top Al-Zn dross samples were mixed with portland pozzolana cement and water of weight 50% mass equivalent of cement to develop top Al-Zn dross/ portland pozzolana cement slabs. The developed top Al-Zn dross/ portland pozzolana cement slabs were further subjected to tests of density, porosity, coefficient of permeability and compressional strength.

Top Al-Zn dross from Roofings Rolling Mills Ltd was composed of mainly aluminium and zinc with traces of other elements combined to form different compounds that are responsible for the variations in the hardness value across its surface. Top Al-Zn dross samples, portland pozzolana cement and water mixture on casting foamed with a noticeable rise in temperature, with porosity confirmed in all the top Al-Zn dross/ portland pozzolana cement slabs. The analysis of top Al-Zn dross/ portland pozzolana cement slabs revealed varied physical properties depending on the amount of top Al-Zn dross added in the mixture, for instance, density, porosity, and permeability increased with further addition while the compressional strength after seven days of curing reduced. The coefficient of permeability of top Al-Zn dross/ portland pozzolana cement slabs varied inversely with the compressional strength. Top Al-Zn dross/ portland pozzolana cement

slabs produced from a mixture containing 39% top Al-Zn dross possessed a combination of both maximum coefficients of permeability and compressional strength.

From the results of the experiment conducted, top Al-Zn dross from Roofings Rolling Mills Ltd can be used as a foaming agent when mixed with portland pozzolana cement and water to develop slabs that can be used for water seepage applications. Further development of top Al-Zn dross/ portland pozzolana cement slabs should be investigated with uniformed sized top Al-Zn dross particles and with the addition of other ceramic materials wastes like broken bricks, tiles, etc. The costs involved in development of top Al-Zn dross/ portland pozzolana cement slabs should be further studied including the analysis of water filtered through them to determine the level of toxicity.

DECLARATION

This thesis document is my own initiative under the guidance and supervision of Dr. Catherine Wandera and Dr. Jerome .B. Ssengonzi. I affirm that the document has never been produced or published in any higher institution of learning for the award of any academic qualification

APPROVAL

This thesis document is solely the work of Mr. Batia Stephen, a student under my supervision and I do acknowledge to the best of my knowledge that this has been his own effort.

Supervisor 1

Sign…….

Dr. Catherine A. Wandera

Supervisor 2

Sign……..

Dr. Jerome B. Sengonzi

ACKNOWLEDGMENT

This document has been authored with the moral support of the Head of Department, Mechanical and Production Engineering of Kyambogo University, Dr. Titus .B. Watmon, and my supervisors Dr. Catherine Wandera and Dr. Jerome .B. Ssengonzi, whose vast knowledge, advice and guidance fortified me with the necessary research and writing skills. I wish to thank the management of Roofings Rolling Mills Ltd and the technical staff for their warm hospitality and support which facilitated my easy data and sample collections. Thanks to Mr. Okumu Lawrence, the material laboratory technician of Kyambogo University for his guidance and expertise in operating the testing equipment and finally Mr. Aleti Abele Emmanuel who sponsored part of the research. I highly regard and appreciate their contribution. God Bless them.

TABLE OF CONTENTS

LIST OF TABLES

LIST OF FIGURES

CHAPTER ONE

1.0 INTRODUCTION

This chapter introduces the study of the byproducts from the galvanizing plant most especially the generation and the chemical composition of dross, with the inclusion of the current strategy employed in the utilization of dross at Roofings Rolling Mills.

1.1 Background

Manufacturing Industries are one of the most significant growth sectors in Uganda's economy creating employment, business through locally manufactured value-added products, and taxes to the government with a contribution of 3.3% to the national gross domestic product (GDP) in 2016/2017 financial year (Uganda Bureau of Statistics, 2018). Roofings Rolling Mills (RRM) Ltd, a member of the Roofings Group, is a leading producer of steel products in Uganda and a big contributor to Uganda's economy, (Roofings Rolling Mills Ltd, 2013). The steel products at RRM Ltd are coated with aluminium-zinc in a galvanization process to get corrosion resistant steel products. The galvanization process at RRM Ltd employs the hot dip bath technology that involves the dipping of carbon steel sheets and other iron based products into a molten bath of aluminium-zinc (Al-Zn) mixture. The galvanization process is the most common industrially applied corrosion protection method because it ensures a fast uniform application of the corrosion resistant layer onto the steel products in an economical way.

While the galvanizing process results in the formation of the desirable Al-Zn coating on the steel products, the reaction of the ferrous oxides (FeO and Fe_2O_3), with the bath contents leads to the formation of galvanizing waste referred to as "dross," which contains ZnFe, ZnAlFe, $ZnFeAl_2O_3$, Fe_2O_3, Al_2O_3 and ZnO (Willis, 2005). The dross formed lowers the quality of the coating layer deposited on the steel products hence the need to avoid its accumulation by periodically scooping it out of the galvanizing bath (Trpčevská *et al*. 2010), besides the removal of the iron ferrous oxide layer from the steel products in the pickling stage. Though the ferrous oxide layer is removed from the steel products during the pickling stage, the iron in dross is traced from further oxidation of the material being coated during their transmission to the galvanizing bath. The dross formed has variable densities as compared to the density of the molten aluminium-zinc metal. The less-dense dross floats and becomes the top dross while the more dense dross sinks

and becomes the bottom dross (Willis, 2005). Top dross was found to consist of mostly AlFe, oxides and chlorides of zinc, with traces of intermetallic compounds (Fe_2Al_5Znx) (Kozlowski and Laskawiec, 2000), (Mader, 2000), while the bottom dross was found to contains Al, Zn, Si, Fe and $FeZn_{10}(\delta)$ (Luo *et al.*, 2013), (Tang, 2000). The quantity and variety of products found in dross have contributed to the characterization of the galvanizing process as a dirty process (Hegewaldt *et al.*, 2001), (Silva *et al.*, 2005). Top dross is harvested by skimming with the inclusion of large amounts of useful metallic aluminium and zinc which is trapped in the harvesting equipment (Vourlias *et al.*, 2007).

The salvaged dross from the galvanizing bath contains metallic zinc in percentage ranges of 40 to 80 % (Barakat, 2003), with the percentage of trapped metallic zinc in dross dependent on the operators' skimming practices (DuBois, 2003). A galvanizing process that generates 18 tons of dross per month containing 70% metallic zinc is reported to make a financial loss of approximately US$40,000 per month if the generated dross is discarded (Mark *et al*. 2007). The quantity of useful products in dross is recoverable and has an economic value, with reported benefits like reduction in the cost of production and prevention of environmental pollution (Mahbubur *et al*., 2013), (Leclerc *et al*. (2002).

The dross generated from the galvanizing process at Roofings rolling Mills Ltd is cast into blocks and sold to industries that have facilities to recycle it. According to (Ainsley, 2012), dross from the galvanization process contains approximately 96 % zinc valued at 75% the cost of special high grade (SHG) zinc. The value generated from the sale of dross by RRM Ltd is not commensurate with the number of valuable products trapped in it. Despite the low income generated from the sale of dross, RRM Ltd continues importing SHG aluminium and zinc ingots for the production of galvanized products and is reflected as an additional cost of production. The usage of SHG aluminium and zinc ingots for the galvanization process results in increased consumption of aluminium and zinc, and increased generation of dross, therefore, necessitating the suggestion of an alternative process that can utilize the abundant dross generated at RRM Ltd.

1.2 Problem Statement

The galvanization process, where a steel sheet is dipped into a molten pool of a mixture of aluminium and zinc, produces dross, a byproduct that contains high percentages of useful aluminium and zinc (Vourlias *et al.,* 2007). The sale of dross generates income that is disproportionate to the number of useful products trapped in dross moreover, steel manufactures engaged in the galvanization process continue with the importation of special high-grade aluminium and zinc ingots for the production of corrosion resistant products (Ainsley 2012). The continuous importation of special high-grade aluminum and zinc ingots coupled with their low-efficiency utilization in the galvanization process raises the quantities of dross generated in the galvanization process. The greater amount of dross generated during the galvanization process necessitates an alternative method of dross utilization.

1.3 Main Objective

To explore the potential of using top Al-Zn dross in the manufacture of pervious slabs as an avenue for utilization of large quantities of dross generated at Roofings Rolling Mills Ltd.

1.4 Specific Objectives

(i) To characterize the top Al-Zn dross generated in the aluminium-zinc galvanizing bath during the hot dip galvanization process at Roofings Rolling Mills Ltd.

(ii) To determine the physical properties of top Al-Zn dross/ portland pozzolana cement slabs made of varying mass proportions of top Al-Zn dross and portland pozzolana cement

(iii) To determine the optimum mass percentage of top Al-Zn dross that can produce top Al-Zn dross/ portland pozzolana cement slabs with a combination of maximum coefficient of permeability and maximum compressive strength.

1.4 Research Questions

(i) What are the chemical and physical properties of top Al-Zn dross from the galvanizing bath at Roofings Rolling Mills Ltd?

(ii) What are the physical properties of slabs made of varying proportions of top Al-Zn dross and portland pozzolana cement?

(iii) What mass percentage range of top Al-Zn dross can produce dross/ Portland pozzolana cement slabs with a maximum combination of both coefficient of permeability and compressive strength?

1.5 Contribution of the Study

The study explores an alternative method of utilization of the large quantities of top Al-Zn dross generated from 55% Al, 43% Zn galvanizing bath in the production of innovative products like porous blocks that can be used for water seepage.

1.6 Justification

Dross contains high percentages (40 to 80%) of useful products that can be used in other processes (Barakat, 2003). Dross generated in quantities of 80 tons per month containing 70% metallic zinc causes a financial loss of US$40,000 per month if discarded (Mark *et al*. 2007) furthermore, the sale of dross generates income that is disproportionate to the number of useful products trapped in dross during the galvanization process (Ainsley,2011).

1.7 The Conceptual Framework

This network shows how the objectives of the study were achieved by relating the variables that are investigated in the study

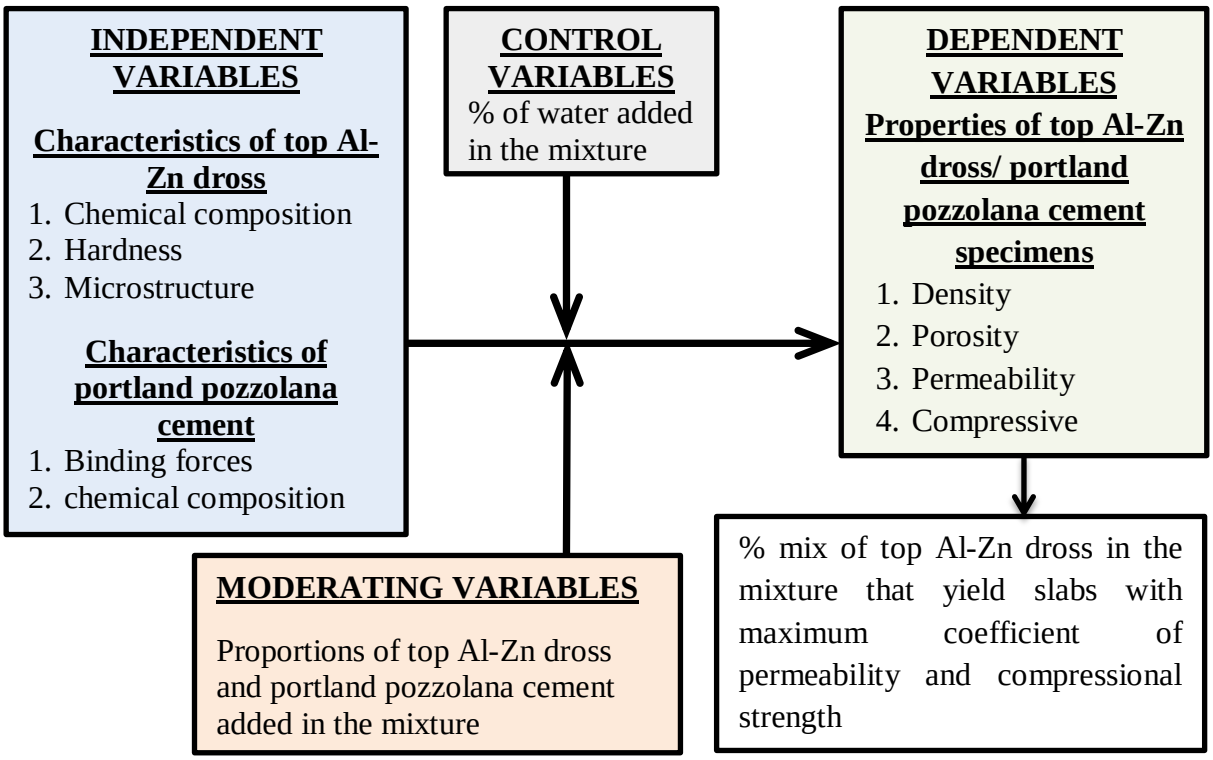

FIG.1- 1 Conceptual Framework

1.8 Scope of Study

The study focused on examining the chemical constituents and physical properties of top Al-Zn dross generated from Roofings Rolling Mills Ltd galvanizing bath, including the physical properties of specimen slabs produced from top Al-Zn dross and portland pozzolana cement. The physical properties of top Al-Zn dross/ portland pozzolana cement slabs namely, density, porosity, water permeability, and compressional strength were studied. Additionally, the determination of the optimum mass percentage of top Al-Zn dross that can be mixed with portland pozzolana cement and water to produce slabs with a combination of the maximum coefficient of permeability and maximum compressive strength was carried out.

1.9 Limitation

A limited amount of top Al-Zn dross was accessed which restricted the casting of standard-sized concrete cubes for testing compressional strength. Smaller cubes, with a lesser dimension as specified by the BS 1881-116: 1983 were cast and used in the experiment. Lack of specialized equipment, like the scanning electron microscope with the x-ray diffraction spectrometer, limited further analysis of the microstructure in terms of determining the phase compositions of top Al-Zn dross.

CHAPTER TWO

2.0 LITERATURE REVIEW

This section presents the characteristics of dross generated in the galvanization process.

2.1 Generation of Dross in the Galvanizing Bath

Bethlehem steel company in1972 patented the galvalume process in which a steel sheet moving at velocity is dipped in a molten bath of 55% Al, 43.5%Zn and 1.5% Si so that the steel sheet is coated with corrosion resistant layer (Murgulescu *et al*. 1965).

During the galvalume process, a process analogous to the continuous galvanization process, byproducts are formed which include dross, spent flux skimming and flue dust. Dross, in particular, composed of oxides and intermetallic compounds, are formed when the molten bath contents react with the atmosphere and iron atoms shed into the hot bath (Marder, 2000), (O'Dell *et al*. 2004), (Willis, 2005). The dross formed is precipitated from the melt when the solubility of iron atoms shed into the molten bath exceeds the saturation solubility of the zinc melt, which is affected by properties like temperature and presence of alloying elements (Nakano, 2002), (Ilinca *et al.* 2007), (Miao, 2005), (Liu and Lin, 2010), (Shawki and Hamid, 2003), (Varadarajan, 2008), (Vourlias *et al.* 2007), (Liberski, 2008). The dross formed segregates into top dross and bottom dross which greatly effects the quality of the galvanized products and the safety of the galvanizing equipment, therefore necessitating its periodic removal from the galvanizing bath (Barakat, 2009), (Kreibich, 2007), (Trpčevská *et al*. 2010).

2.1.1 Top Dross

Top dross, density floats on top of the galvanization melt and is harvested from the galvanizing bath during an ongoing galvanization process (Dong *et al.* 2008). The top dross during the galvanization process may get trapped between the steel substrate and the coating layer to form defect visible on the surface of the coated material referred to as "the coating pimple" (Horstmann, 1975), (Avik *et al.* 2018). The removal of the top during an ongoing galvanization process is possible because the operators of the galvanizing bath can easily access and remove the top dross from the bath using special shovels.

2.1.2 Bottom Dross

The bottom dross sinks and in the process collides with the sink rolls, eventually settling on the floor of the galvanizing kettle (Marder 2000), (Gagné *et al.* 1992). Bottom dross is a poor conductor of heat which causes localized overheating and if not removed and may escalate into the development of holes onto the galvanizing bath material and or, causes the impairment of the sink rolls, affecting their proper functioning (Ainsley 2012), (Gagné *et al,* 1992). Unlike top dross, bottom dross is harvested when the process is shut down, the bottom dross harvested is recycled, sold or disposed of in accordance with the set disposal procedures set by environmental bodies to avert the risk of environmental pollution (Turan, 2004), (Alane *et al*, 2008).

2.2 Characterization of Dross from the Galvanizing Bath

The characterization of dross is based on the chemical composition, physical characteristics displayed when treated in a particular manner and the microstructure as viewed under a light microscope.

2.2.1 Chemical Composition of Dross

Top dross from a galvanization process is composed of oxides and chlorides of zinc and aluminium, with traces of intermetallic compounds of Fe_2Al_5Znx or Fe_2Al_5-xZn_x, (Marder, 2000), (Liu *et al.* 2002). The Scanning Electron Microscope analysis (SEM) shows high percentages of oxygen, zinc, and aluminium with a concentration of 58%, 20.2%, and 14.7% respectively, and traces of carbon, chlorine, lead, iron, and tin, (Vourlias *et al*. 2007). The process of harvesting dross by skimming collects large amounts of un-utilized coating materials that are trapped in the harvesting equipment hence the reason for larger amounts of metallic zinc in dross (Vourlias *et al.* 2007). From the studies by (Luo *et al*. 2013) using the electron discharge spectrometer, bottom dross contained Al, Zn, Si, and Fe in all samples collected at different temperatures. (Tang, 2000) observed $FeZn_{10}$ in bottom dross while (Trpčevská *et al*. 2010) identified $FeZn_{13}(\zeta)$. Bottom dross is made up of the intermetallic particles of zinc-iron (ZnFe), whose chemical composition and quantity precipitated depends on the temperature and composition of the bath (Marder, 2000), (Liu *et al*. 2002), (Maass and Peissker, 2011). The high quantities and varieties of wastes generated from the hot dip galvanization process have led to its

categorization as a dirty process, hence the difficulty in defining the chemical composition of dross (Hegewaldt *et al*. 2001), (Silva *et al*. 2005), (Trpčevská *et al.* 2010).

2.2.2 Microstructure of Dross

The microstructure of a metallic specimen can be observed after it has been prepared through stages like cutting, grinding, polishing, etching in a suitable acid and rinsing in a non-reactive solvent. The cutting process should not induce microstructural changes in the specimen, the polished surface should not contain any visible scratches and the etching process should be closely monitored to a point that reveals the required details (Goodhew, 1973), (McCall *et al*. 1974), (American Society for metals 1972), (Vander Voort, 1984).

Studies have shown that the microstructure of aluminium zinc alloys appears as in Fig. 2-1 when etched in copper sulphate ($CuSO_4$) solution in a concentration of 200 g per liter.

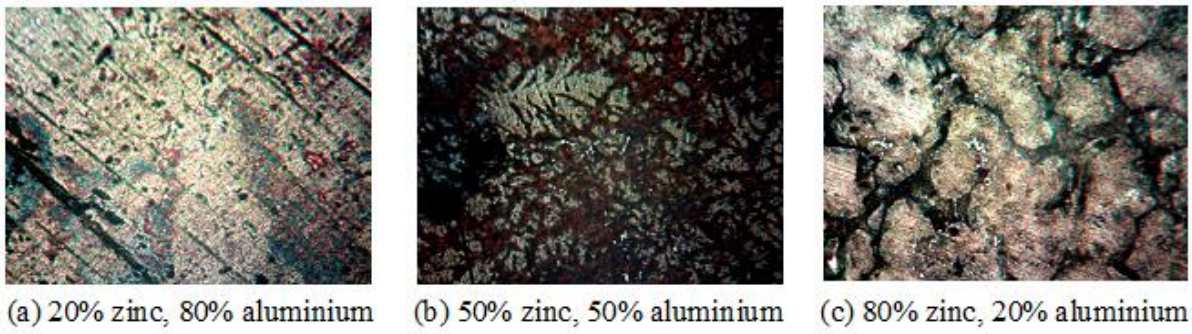

FIG. 2- 1 Microstructure of Zn-Al alloy system
(Source: Fajardo *et al.*, 2014)

2.3 Extraction of Useful Products from Dross

The research works conducted on recycling and utilization of dross to produce an end product is aimed at maximizing the economic benefit, besides containing and preventing the dispersion of toxic compounds into the environment (Cook, 1997). The extraction of useful elements from galvanization byproducts is possible, with recovery efficiency dependent on the environmental and service conditions a metal is subjected to during its service life and the manufacturing process (Rabah and El-sayed, 1995). Pyrometallurgical, hydrometallurgical or combination of

both processes has been used in the extraction of useful products from dross, with the pyrometallurgical recovery process most applied in the recovery of metallic zinc.

2.3.1 Pyrometallurgical Processing of Dross

The pyrometallurgical process is used to extract zinc and its compounds from secondary zinc sources either by distillation and sublimation in an inert environment or through the oxidation of zinc vapor in oxygen to obtain zinc oxide using muffle furnaces, Larvik furnaces, bottle retorts, etc. (Everitt, 2006), (Paul & Queneau, 2015). When dross is heated to temperatures of 450°C and above, zinc melts and can be collected, a principle behind the development of the Metalullix Zincoff Recovery (MZR) system, with optimum zinc recovery temperatures of below 600 °C (Paul & Queneau, 2015). The yield of zinc from the pyrometallurgical process is dependent on temperature, use of fluxes, duration of heating, the particle size of dross, etc., producing residues that contain low amounts of zinc in sufficient quantities that can be reprocessed to valued products (Barakat, 2003), (Paul & Queneau, 2015).

2.3.2 Hydrometallurgical Processing of Dross

The hydrometallurgical process is suitable in processing low zinc-containing materials and the process is considered more eco-friendly than the pyrometallurgical processes (De-Wet & Singleton, 2008). Among the hydrometallurgical methods used for extraction of zinc from dross, solvent extraction (which selectively recovers heavy metals like zinc, copper, cadmium, and Nickel) was proposed (Elżbieta *et al*. 2015), (Martin *et al.* 1983). The recovery of zinc by electro-winning without the addition of alkali requires the removal of iron from the dissolved liquor (Agatzini-Leonardou *et al.* 2000). The hydrometallurgical process filtrates contain zinc whose concentration increases either with an accumulation of the pile or due to incomplete leaching of the dross with low acid concentration as a consequence of overutilization of the leaching acids (Ozverdi, and Erdem, 2010), (Min-xiao-bo *et al.* 2013).

2.3.3 Pyro-Hydrometallurgical Processing of Dross

Though the pyrometallurgical and hydrometallurgical processes are successful in the extraction of useful products, their residues contain traces of zinc which are a potential environmental

hazard. High extraction rates can be achieved by a combination of pyrometallurgical and hydrometallurgical processes, involving residue concentration steps like sorting of metallic from nonmetallic (Paul & Queneau, 2015). High-efficiency extraction of zinc from zinc leaching residue was reportedly achieved by leaching at high temperatures of about 90°C and in high acid concentrations, with reported increased solubility of ZnFe (Coupur *et al.* 2004), (Leclerc *et al.* 2002), (Zheng-gwang *et al.* 2015).

Though pyro-hydrometallurgical processes have been developed to contain zinc leaching residue, their filtrates contain traces of zinc which is an environmental hazard if poorly handled, with negative effects on plants and animals (Halloway *et al*. (2007). The water-soluble zinc causes soil contamination, water pollution through the leachate by rainfall originating from damped wastes in landfills (Özverdi and Erdem 2010). Therefore, it is necessary to utilize dross in the development of products that ensure a reduction or complete lockdown of hazardous materials to avoid their dispersion into the environment.

2.4 Utilization of Dross in Production of Porous Concrete Components

Concrete, the most widely used construction material that is subjected to several extreme stress conditions during service, is obtained by mixing cement, water, and aggregates**.** When cement is mixed with water, a reaction is initiated that results in the formation of a solid with pores, which implies that there are pores in concrete. The pores in concrete are due to the evolution of gases due to the reaction of the constituents making up the concrete and inadequate compaction. The pores developed reportedly affect the properties of concrete most especially the strength and porosity (Nagraj and. Zahida 1996), (Da¨rr, and Ludwing 1973), (Rostasy *et al.* (1980). The process of coming up with a concrete mix design involves choosing suitable ingredients and determining their relative quantities in producing the most economical concrete while retaining properties such as strength, durability, and consistency (Vipin *et al.* 2017).

The utilization of waste containing high alumina as a replacement for fine aggregates in producing cement mortar resulted in products with increased total porosity, decrease in mechanical strength as compared to the conventional silica sand mortar concrete (Puertas, Blanco & Vasquez). The desirable properties of concrete like strength, workability, durability,

resistance to cracks and permeability can be enhanced by the addition of some pozzolanic materials (Vikas *et al.* 2012), (Nooman, 2016).

2.4.1 Porosity in Cement-Dross Components

Concrete pores developed during the process of manufacture differ depending on the rate of compaction. The pores developed in a well-compacted mortar are different from the pores developed in a non-compacted mortar though prepared using identical proportions of the same ingredients (Winslow and Liu, 1990), (Reinhardt *et al*. 1995). The porosity and Strength of concrete also depend on the water-cement ratio, with practical limits of water-cement ratios of 0.38–0.65 (Rakesh and Bhattacharjeeb, 2003). Porosity in concrete can be enhanced by the addition of a predetermined amount of aluminium powder and other additives into a slurry of ground silica sand cement or lime in a process termed as autoclaved aerated concrete, (Yen, 2006).

The porosity and low density in aerated concrete are caused by the evolution of hydrogen bubbles from the reaction between calcium hydroxide from cement and aluminium powder, as in the equation (2-1) (Mobasher, 2012), (Barber, 1972). The use of greater amounts of foaming agents causes the release of bubbles resulting in wider pore distribution leading to a lower strength. The rate of the evolution of the gas bubbles determines the success of the aerated product (Holt and Ravio, 2005).

$$2Al + 3Ca(OH)_2 + 6H_2O \rightarrow 3CaO.Al_2O_3.6H_2O + 3H_2 \qquad (2-1)$$

2.4.2 Permeability

The permeability of a material, the ability to allow the passage of fluids through it under the action of differences in pressure, is influenced by properties like the size, distribution and the type of cavity created (cavities that are open-ended allow uninterrupted flow of water while those that are closed are barriers to fluid flow) (Yen, 2006). The permeability of porous concrete is facilitated by the presence of open pores. Concrete with closed pores is used mainly in thermal & sonic insulation or in areas where low specific gravity structural components are required (Sulaiman, 2011). The environmental effects of liquid and gaseous substances have a negative

effect on the serviceability of concrete hence knowing its permeability allows the assessment of its durability (Tracz, 2016).

2.4.3 Compressive Strength of Concrete Products

The strength of concrete is determined by the properties of the ingredients (constituent materials), the mix proportions, and the method of compaction used in the manufacturing process. Cement, the binding material in concrete, is manufactured from lime, silica, alumina and iron oxide which interact at high temperatures in a kiln to form a complex compound. Concrete of low porosity that is well bond with a reliable bonding material (such as Portland cement) produces high compressive strength concrete (Schiller, 1971). The various properties of cement are influenced by the relative proportion of each of the constituent oxides, the rate of cooling, and the fineness of the grains.

CHAPTER THREE

3.0 METHODOLOGY

This chapter constitutes the methods that were used to determine the objectives of the study.

3.1 Characterization of Top Al-Zn Dross Generated in a Galvanizing Process at RMM Ltd.

Top Al-Zn dross was harvested at different intervals from the galvanizing bath during an ongoing continuous galvanizing process as illustrated in FIG. 3-1, and later characterized in terms of the chemical composition, microstructure, and hardness.

FIG. 3- 1 Harvesting of top Al-Zn dross during an ongoing galvanizing process

3.1.1 Preparation of Top Al-Zn Dross Samples

The top Al-Zn dross was extracted from the galvanization bath after every three-day interval so that a total of five samples were obtained. One specimen was prepared from each of the five samples of the top Al-Zn dross, with one shaped after cooling a solid mass of top Al-Zn dross by cutting using a power saw (FIG. 3-2), while the remaining four were cast in a cone-shaped mold giving a total of four cone-shaped specimens. The specimens of top Al-Zn dross were marked A, B, C, D and E (FIG. 3-3).

FIG. 3- 2 Cutting the top Al-Zn dross samples with a power saw

FIG. 3- 3 Specimens obtained from top Al-Zn dross samples extracted at different intervals.

3.1.2 Chemical Analysis of Top Al-Zn Dross

The top Al-Zn dross specimens were polished using an automated sanding machine mounted with a fine sanding paper of grit number 360 until a flat, uniform surface was obtained (FIG. 3-4). The chemical composition of the top Al-Zn dross specimens was analyzed using the spark absorption spectrometer (Model name: SpectroMax X), with each of the five top Al-Zn dross specimens tested three times at different spots on the polished surface (FIG. 3-5). The results obtained were annexed in Appendix.1-1 to 1-5.

FIG. 3- 4 Specimen Preparation

FIG. 3- 5 Specimen mounted on the spark absorption spectrometer for analysis

3.1.2 Analysis of Hardness

The Rockwell's hardness testing machine model name (HOYTOM) was used to determine the hardness of dross according to the ASTM E18-11 standards. The top Al-Zn dross specimens were cut to size using a hacksaw (FIG. 3-6), and the surface to be subjected to the hardness test cleaned with soap and water to remove dirt and oil. Each cleaned specimen was mounted on the hardness testing machine one at a time and tested five times at different spots on the cleaned surface using a diamond indenter with the pre-load set to 10kgf and main load set to 150kgf (FIG 3-7). The results of the hardness test were taken from the HRC scale after the indicator had stopped moving and the main load removed and were tabulated as recorded in TABLE 4-2.

The procedure used to determine the hardness of the top Al-Zn dross specimen was replicated in the determination of the hardness of the mild steel, so as to compare the hardness of both materials. Each of the three specimens of mild steel marked X, Y, and Z were tested five times at different spots on the surface and the results tabulated as shown in TABLE 4-3.

FIG. 3- 6 Cutting the top Al-Zn Dross specimen to size using a hack saw

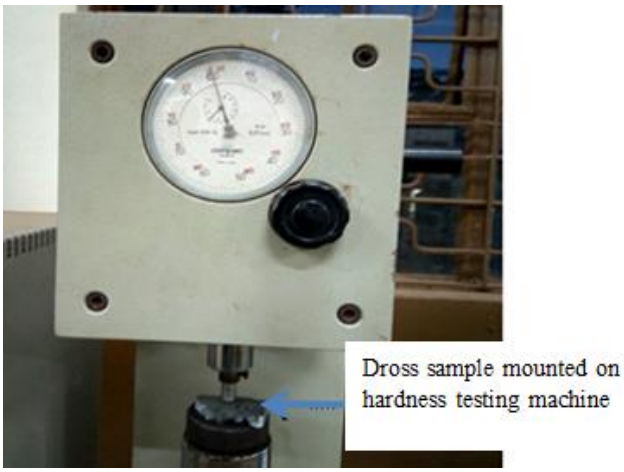

FIG. 3- 7 Hardness testing of top Al-Zn dross sample

3.1.3 Analysis of Microstructure of Top Al-Zn Dross

Three of the top Al-Zn dross specimens (used in hardness testing experiment) were selected for microstructural analysis (specimen A, C, and E). The surface of the specimen to be examined

was polished using a polishing machine (shown in FIG. 3-8), through four polishing cycles while varying the revolution of the polishing wheel from 50 to 500rpm.

Polishing was initially performed on polishing wheels mounted with a coarse sanding paper of abrasive number 120 and later on replaced with finer sanding paper of abrasive number 320 and 480 respectively. The polishing operation was finalized on a micro cloth with 0.05 μ Gama alumini applied on the wet surface medium ensured by the constant flow of water through the water nozzles of the polishing machine.

After polishing and when no scratches were visible by the naked eye, the polished surface was etched in a solution made of 98 % ethanol and 2 % nitric acid, dried and mounted on the KRUSS metallurgic optical microscope with a digital optical lens (FIG. 3-9). The photographs of the microstructural images were taken and appeared as in FIG. 4-1.

FIG. 3- 8 Polishing machine

FIG. 3- 9 The Kruss optical microscope

3.2 Determination of the Physical Properties of Top Al-Zn Dross/ Portland pozzolana Cement Slabs

This section contains the procedure that was used to develop and determine the physical properties of top Al-Zn dross/ portland pozzolana cement made of varying proportions of dross and cement respectively.

3.2.1 Development of Top Al-Zn Dross and Portland pozzolana Cement Slab Specimens

All the materials used in the manufacture of top Al-Zn dross/ portland pozzolana cement slabs were sourced locally in Uganda, namely; water from Uganda National Water and Sewage Corporation, portland pozzolana cement from Tororo cement, sourced from a local hardware store and top Al-Zn dross from RRM Ltd, harvested during and ongoing galvanization process. The particle size of the top Al-Zn dross was reduced mechanically by beating with a sledgehammer when hot, cooled in natural air and sorted according to size using a sieve, with K having particle size of less than 1mm, L with particle size range of less than 5mm and greater than 1mm, M with particle size range of less than 10mm and greater than 5mm (FIG.10). The top Al-Zn dross used in developing the top Al-Zn dross/ portland pozzolana cement slabs was prepared by mixing the different particle sizes K, L, and M in mass ratios of 5: 3: 2 respectively.

(a) Beaten dross sample (b) Sorted Dross samples

FIG. 3- 10 Preparations of top Al-Zn dross samples

Top Al-Zn dross, portland pozzolana cement, and water were measured using an electronic weighing scale as shown in Fig 3-11. The top Al-Zn dross and Portland pozzolana cement were thoroughly mixed in mass percentage ratios of 10:90, 20:80, 30:70, 40:60, 50:50 to get top Al-Zn dross and portland pozzolana cement mixture which was used in the development of the

concrete mix design F, G, H, I and J respectively. The mass of water added in the top Al-Zn dross/ portland pozzolana cement mixture was equivalent to 50% the mass of the portland pozzolana cement. The combined ingredients of top Al-Zn dross, portland pozzolana cement, and water were thoroughly mixed and immediately cast into wooden molds (to allow subsequent reactions to take place in the mold) without ramming to come up with fifteen (15) top Al-Zn dross/ portland pozzolana cement slabs, made from each of the concrete mix design F, G, H, I and J as represented in TABLE 3-1. After 48 hours of setting away from direct sunlight and at room temperature, the specimens were removed from the mold awaiting further analysis as shown in Fig 3-12.

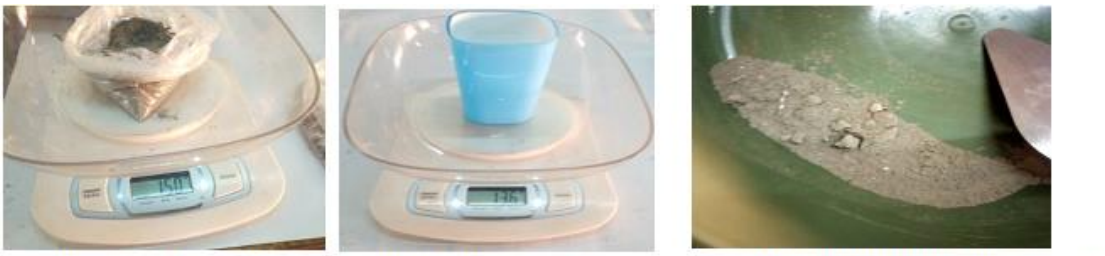

(a) Mass of cement (b) Mass of water (c) Mixture of Dross and cement

FIG. 3- 11 Cast specimen preparation.

FIG. 3- 12 Concrete specimens used for determination of density and porosity

TABLE 3- 1 Top Al-Zn dross/ portland pozzolana cement cast specimen mix design combinations

Concrete design mix	Top Al-Zn dross/ cemet slab	Top Al-Zn dross		Portland pozzolana Cement		Water
		Mass of Al-Zn dross M_d (g)	Weight % of Al-Zn dross (%)	Mass of portland pozzolana Cement M_c (g)	Weight % of portland pozzolana Cement (%)	Mass of Water Equivalent to 50% Mass of portland pozzolana Cement M_w (g)
F	F1	30	10	270	90	135
	F2	30	10	270	90	
	F3	30	10	270	90	
G	G1	60	20	240	80	120
	G2	60	20	240	80	
	G3	60	20	240	80	
H	H1	90	30	210	70	105
	H2	90	30	210	70	
	H3	90	30	210	70	
I	I1	120	40	180	60	90
	I2	120	40	180	60	
	I3	120	40	180	60	
J	J1	150	50	150	50	75
	J2	150	50	150	50	
	J3	150	50	150	50	

.

3.2.2 Determination of Density of Top Al-Zn Dross/Cement Slabs

The determination of density was based on the ASTM: C 567 – 00 Standard. The determination of oven density was carried out on cube-shaped specimens. The oven density of porous concrete was determined by calculation.

The oven-dry density of the top Al-Zn dross/ portland pozzolana cement slab was calculated using the expression:

$$O_\delta = \frac{(M_d + 1.2M_c)}{V} \qquad (3-1)$$

Where: O_δ = oven density as calculated in kg/m^3

M_d = the mass of top Al-Zn dross, kg,

M_c = the mass of Portland pozzolana cement, kg,

M_W= the mass of water, kg

$\boldsymbol{V}$ = the volume calculation of the cube-shaped slab obtained using the dimensions of the cube, length *L1*, width *L2*, and Height *L3*, measured using Vanier calipers as illustrated in **Fig** 3-13,

$$\boldsymbol{V} = L1 \times L2 \times L3 \qquad (3-2)$$

The results of the calculated oven density were tabulated and annexed in Appendix 2.1.

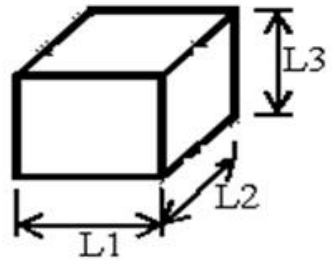

(a) Sketch depicting the measured lengths of the sides of the cube shaped cast slab

(b) Measuring the specimen using a Vanier caliper

.

FIG. 3- 13 Measurement of the specimen dimensions using a Vanier caliper

3.2.3 Determination of Porosity of the Top Al-Zn Dross/ Portland pozzolana cement Slabs

The specimen samples used in the determination of density were used to determine the porosity; therefore their volumes are the same. The top Al-Zn dross/ Portland pozzolana cement specimens were placed in a laboratory environment at a temperature of 25℃ and away from direct sunlight for 72 hours before the commencement of the experiment. Using a weighing scale, the mass of the top Al-Zn dross/ Portland pozzolana cement specimen when in air and when submerged in water was determined as shown in FIG. 3-14. The results were calculated to get the open porosity using equation (3-3), as applied by the researcher, Rama and Shanti, 2015, and annexed in Appendix 3.1

$$Vr = 1 - \left(\frac{W2-W1}{\delta wV}\right) \times 100 \qquad (3-3)$$

Where:- *Vr* = porosity (%),

- *W1* = weight under water (g),
- *W2* = oven dry weight (g),
- *V* = volume of sample (m^3) and,
- δw= density of water (g/m^3).

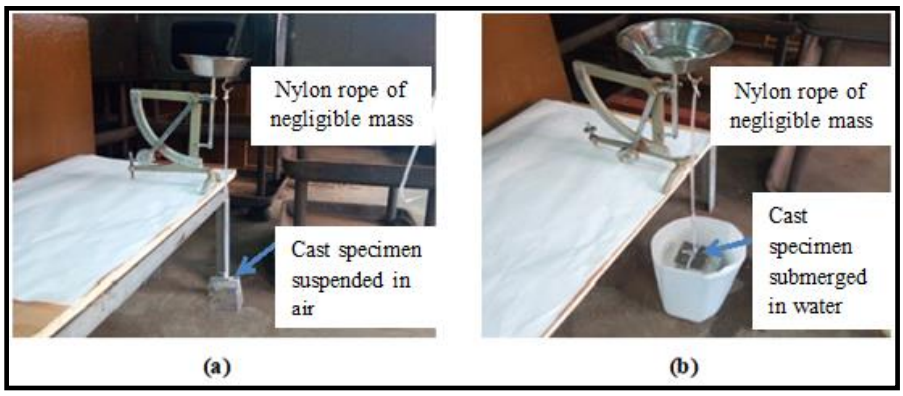

FIG. 3- 14 Measurement of the mass of the top Al-Zn dross/ portland pozzolana cement slabs

3.2.4 Determination of Coefficient of Permeability of Top Al-Zn Dross/ Portland pozzolana Cement Slabs

The determination of permeability, the ability to allow the flow of water through a sample by creating different pressures on either of its faces of porous materials was established using Darcy's law (as in equation 3-5) The applied pressure, that allows the flow of water through the specimen was maintained constant by ensuring a constant head pressure as in shown in FIG. 3-15

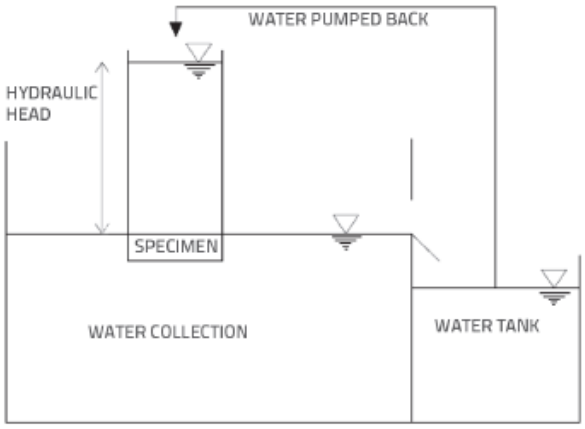

FIG. 3- 15 Experimental test setup based on the constant head pressure
Source: (Rama and Shanthi, 2016)

Another set of fifteen top Al-Zn dross/ portland pozzolana cement slabs were cast with three slabs each from concrete mix design F, G, H, I and J and labeled W1 to W3, V1 to V3, U1 to U3, T1 to T3, and S1 to S3 respectively. After 7 days of curing in a laboratory atmosphere at a temperature of 25℃ and away from direct sunlight, the length L1, width L2, and the height L3 of the Al-Zn dross/ Portland pozzolana cement specimen were measured using Vanier caliper (FIG. 3-13).

The edge of the top Al-Zn dross/ portland pozzolana cement specimen along height L3 was sealed with a combination of vaseline, polyethylene sheet, and rubber codes to act as gasket sealant to only allow the flow of water through the cross-sectional area (L1×L2) of the specimen (FIG. 3-16). The specimen was then placed in the permeability test equipment that was locally fabricated and secured with bolts mounted on the flanges (FIG. 3-17). The complete assembly of the permeability test equipment appeared as in FIG. 1-8

Water from the utility tap, connected through the hose pipe was allowed to flow into the main gallery of the test equipment and after 10 minutes, when a constant flow rate was attained and there was no leakage observed from and through the joint flanges, water seepage through the specimen was collected for 30 minutes. The water collected was measured using a measuring cylinder and the permeability coefficient determined using Darcy's law as in equation (3-4).

$$k = \frac{Q\,h}{AHT} \qquad (3-4)$$

Where, k = the permeability coefficient (mm/s);

Q = the water quantity (mm3) in the t time;

h = the specimen height (mm);

H = the mean water level difference (water head) (mm);

A = the specimen sectional area (mm2); and

t = time (s).

The results obtained from the calculation of porosity was tabulated and annexed in Appendix 4.1

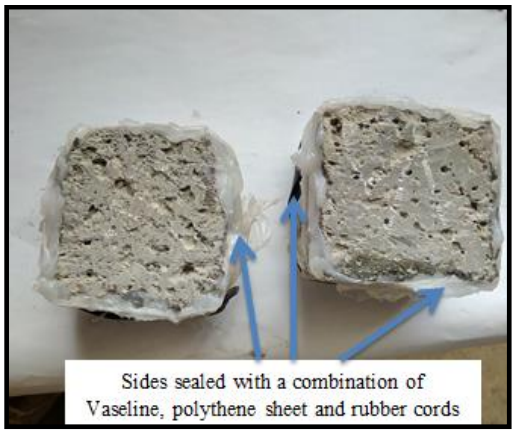

FIG. 3- 16 Sealed edges along the height L3 of the specimen

(a) Specimen fixed in the testing

(b) Specimen secured inside the testing equipment

FIG. 3- 17 Specimens secured in the permeability testing equipment

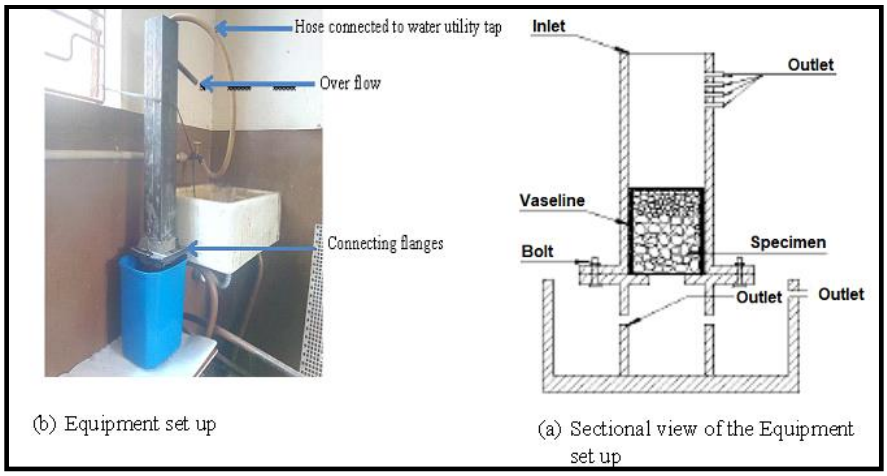

FIG. 3- 18 Experimental set up for the determination of the coefficient of permeability

3.2.5 Determination of Compressive strength of the Al-Zn dross/ Portland pozzolana Cement Slabs

The compressive test is carried out on the hardened cube or cylindrical concrete specimens that must be soaked in water prior to testing after curing for 7, 14 and 28 days according to (BS 1881-116: 1983) Compressive Strength is calculated from the expression

$$Cs = \frac{P}{A,} \qquad (3-5)$$

Where: P = Ultimate compressive load of concrete (KN)

A = Surface area in contact with the platens (mm^2) (i.e. for 100×100)

Compressive strength tests were conducted on the top Al-Zn dross/ Portland pozzolana cement specimens that were used in the determination of the coefficient of permeability which had been cured for seven days. The cubes were completely immersed in water for 24 hours prior to the start of the experiment (FIG.3-19). The compressional strength of the top Al-Zn dross/ Portland pozzolana cement specimen was determined using Denison compressional testing machine, model T.42B4 of capacity 500KN with the compressional load set to 10kg (FIG. 3-20). The cast specimen slabs were placed between two flat steel plates that were large enough to completely cover the cross-sectional area of the top and bottom surfaces through which a compressional force was directed to the top Al-Zn dross/ portland pozzolana cement specimen until

deformation. The deforming force was recorded and the compressional strength calculated using equation (3-5). The calculated results were tabulated and annexed in Appendix 5.1.

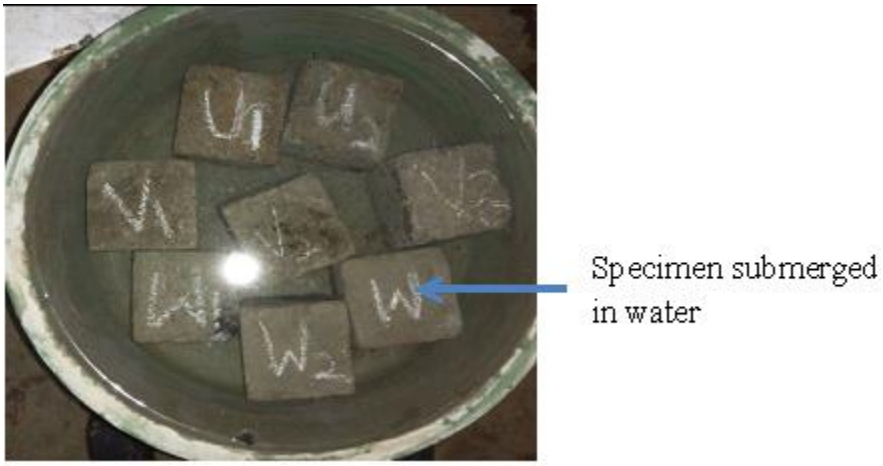

FIG. 3- 19 Soaking of the specimen 24 hours before conducting the experiment

FIG. 3- 20 Denison compressional testing machine, model T.42B4, capacity 500KN

3.3 Determination of the optimum mass of Top Al-Zn Dross in the Top Al-Zn Dross/ Portland Pozzolana Cement Mixture

The data from the experiment used to determine the coefficient of permeability and the data used to determine the compressional strength of the top Al-Zn dross/ portland pozzolana cement slabs were plotted against the same axis of the mass percentage of dross. Trend lines for each parameter of the coefficient of permeability and compressional strength were constructed and forecast to establish their intercept using Microsoft Excel. The optimum percentage mass of top Al-Zn dross required to produce top Al-Zn dross/ portland pozzolana cement slabs with a maximum coefficient of permeability and maximum compressional strength was read at the point of intercept of the trend lines.

CHAPTER FOUR

4.0 RESULTS AND DISCUSSION

The results from the experiments were analyzed by comparison and statistical tools to come up with logical relationships between the independent and dependent variables to explain the observed trends.

4.1 Characterization of Top Al-Zn Dross from RMM Ltd.

The chemical composition, the Hardness and the Microstructure were the parameters studied to characterize top Al-Zn dross sourced from Roofings Rolling Mills Ltd.

The main chemical constituents of top Al-Zn dross are Al with a percentage concentration range of 42 to 55.6%, Zn with percentage concentration range of 42.92 to 61.5 % and Fe, with concentration percentage greater 0.14%. The Al and Zn are the primary coating material while Fe is traced from the steel substrate galvanized. The high concentration percentages of Al and Zn in top Al-Zn dross are due to their inclusions during the extraction process of top Al-Zn dross using special shovels. Other traceable elements, with low concentrations like; Cu, Pb, Cd, and Mg are probably the alloying elements in steel or impurities in SHG aluminium and zinc. The results of the chemical composition with inclusion of the percentage mean distribution of each element in the top Al-Zn dross is summarized across the row in TABLE 4-1. The “A” in TABLE 4-1 is an indication of non-conclusive results due to flaws on top Al-Zn dross surfaces like pores or non-metallic inclusions like char.

The experimental value of HRC determined by Rockwell’s hardness test at different points on the aluminium zinc dross specimen varied significantly as recorded in TABLE 4-2. The chemical analysis by the spark absorption spectrometer confirms the existence of Al, Zn, Fe besides elements with low concentrations (Pb, Cd, and Mg) shown in TABLE 4-1. Aluminium and Zinc are reactive metals at high temperatures therefore, the galvanization process together with various elements present in galvanizing bath created an optimum environment for the formation of various compounds that have different hardness values.

The comparison of the results of the hardness value of top Al-Zn dross from TABLE 4-2 with the results from the hardness test of mild steel in TABLE 4-3 indicates that mild steel is harder than top Al-Zn dross.

TABLE 4- 1 Chemical composition of top Al-Zn dross

Sample	**Tests**	**Elements and their % Concentrations**						
		Al	**Zn**	**Fe**	**Cu**	**Pb**	**Cd**	**Mg**
A	**1**	-	61.5	-	A0.57	A0.008	A0.008	A0.015
	2	A37.13	61	A0.14	A0.21	A0.007	A0.002	A0.014
	3	A46.47	51.6	A0.14	A0.12	A0.004	0.007	A0.012
	mean	A39.97	54.9	A0.14	A0.30	A0.006	A0.003	A0.014
B	**1**	54.4	43.99	>0.14	< 0.100	0.003	0.0003	0.030
	2	52.3	46.08	>0.14	< 0.100	0.003	0.0004	0.004
	3	54	44.39	>0.14	< 0.100	0.002	0.0005	0.003
	mean	53.5	44.82	>0.14	< 0.100	0.003	0.0004	0.004
C	**1**	53.8	44.75	>0.14	< 0.100	0.002	0.0002	0.002
	2	53.8	44.41	>0.14	< 0.100	0.003	0.0003	0.003
	3	55.6	42.97	>0.14	< 0.100	0.002	< 0.0002	0.002
	Mean	54.4	42.06	>2.17	< 0.053	0.003	0.0002	0.003
D	**1**	49.63	48.75	>0.14	< 0.100	0.003	0.0004	0.004
	2	55.4	42.92	>0.14	< 0.100	0.002	0.0003	0.003
	3	53.3	45.13	>0.14	< 0.100	0.002	0.0004	0.003
	Mean	52.8	37.76	> 8.03	< 0.052	0.002	0.0004	0.003
E	**1**	A47.41	50.6	A0.14	< 0.100	A0.006	0.0008	A0.012
	2	46.10	52.3	A0.14	< 0.100	A0.003	0.0007	A0.010
	3	42.00	56.5	A0.14	< 0.100	A0.003	0.0006	A0.010
	Mean	A45.17	36.75	A 16.55	< 0.070	A0.004	0.0007	A0.011

TABLE 4- 2 The HRC value of top Al-Zn dross

Al-Zn Dross Samples	Hardness value				
	1	2	3	4	5
A	HRC 75.1	HRC 82.9	HRC 89.4	HRC 95.0	HRC 93.8
B	HRC 74.8	HRC 91.7	HRC 92.0	HRC 78.0	HRC 88.0
C	HRC 98.0	HRC 72.4	HRC 99.0	HRC 85.0	HRC 77.2
D	HRC 82.9	HRC 98.4	HRC 95.0	HRC 99.2	HRC 78.2
E	HRC 91.8	HRC 80.0	HRC 71.2	HRC 87.4	HRC 92.7

TABLE 4- 3 The HRC values of mild steel

Steel samples	Hardness value				
	1	2	3	4	5
X	HRC 32.9	HRC 37.3	HRC 29.9	HRC 35.5	HRC 30.4
Y	HRC 34. 1	HRC 27.2	HRC 28.9	HRC33.8	HRC 34
Z	HRC 31.2	HRC 32	HRC 29.6	HRC34.8	HRC32.3

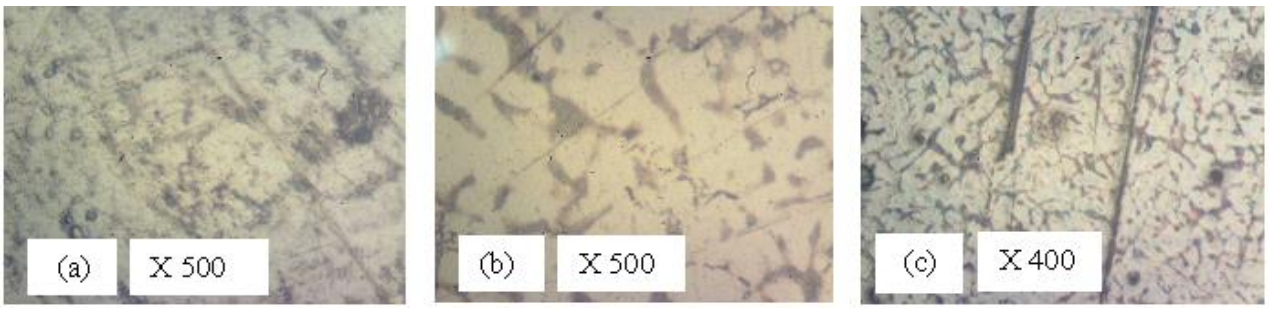

FIG. 4- 1 Microstructure of top Al-Zn dross specimens as viewed with the Kruss Optical Microscope

The image from the microstructural analysis of the top Al-Zn dross samples was as shown in FIG. 4-1. The comparison of the micrograph in FIG. 4-1with the micrograph in FIG. 2-1 revealed a similarity between FIG. 4-1, FIG. 2.1(a) and FIG. 2.1(b). The difference between the micrographs was noted in the number of black spots, which appear less in FIG. 2.1(a), and more

in FIG. 2.1(b) as compared to FIG. 4-1, which according to (Fajardo and Henao,2014) show traces of zinc.

4.2 Observations Noted During Top Al-Zn Dross / Portland Pozzolana Cement Specimen Casting

The amount of force required to reduce the size of top Al-Zn dross by beating was high when the top Al-Zn dross specimen was cold and low when hot. Top Al-Zn dross is hard when cold but becomes soft and brittle when hot because high temperatures cause changes in its microstructure from fine-grained structures to coarse-grained structure.

A few minutes after casting, the formation of bubbles was observed mostly in cast specimen design F, followed by G, H, I and least in J respectively, accompanied by a noticeable rise in temperature as felt by touching the exterior surface of the wooden mold. The bubbles were due to the evolution of hydrogen gas when aluminium in the top Al-Zn dross reacted with calcium oxide in portland pozzolana cement according to the reaction equation (2.1).

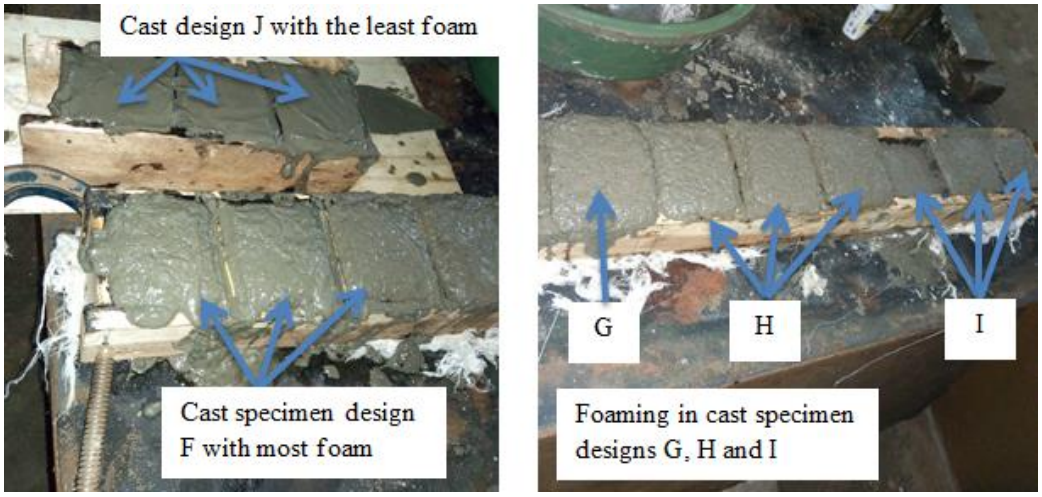

FIG. 4- 2 Foaming in different concrete designs

4.3 Variation of Density of Slab with Mass of Top Al-Zn Dross in the Concrete Mix

TABLE. 4-4 is a summary of the results extracted from Appendix 2.1

TABLE 4- 4 Mass of top Al-zn dross and the corresponding oven-density

Mass of top Al-Zn dross Md (g)	Top Al-Zn dross/ portland pozzolana cement slab	Oven density of top Al-Zn dross/ portland pozzolana cemet, $O\delta \times 10^4 (g/m^3)$
30	F1	146.9
	F2	146.9
	F3	147.5
60	G1	156.05
	G2	153.3
	G3	161.86
90	H1	146.78
	H2	171.86
	H3	171
120	I1	188.76
	I2	158.49
	I3	168
150	JI	160.19
	J2	169.23
	J3	208.86

The variation of density of the top Al-Zn dross/ portland pozzolana cement slab with changes in the mass of top Al-Zn dross is illustrated by the graph in FIG. 4-3. The graph shows that increase in the mass of top Al-Zn dross in the mixture increases the density of top Al-Zn dross/ portland pozzolana cement slab. The increase in density is due to the increase in the number and size of voids in the top Al-Zn dross/ portland pozzolana cement slab. The increased number of voids created is attributed to the increase in the reactive aluminium in dross which resulted in an increased chemical reaction and evolution of hydrogen gas.

FIG. 4.4 shows the extent to which the increase in the mass of top AlZn dross affects the variations in the density of the cast top Al-Zn dross/ portland pozzolana cement specimen. The coefficient of determination $R^2 = 0.454$ indicates that 45.4 of the changes in the density can be explained by the relationship. A positive gradient indicates that an increase in the mass of top Al-Zn dross in the mixture increases the density of top Al-Zn dross/ portland pozzolana cement cast specimens.

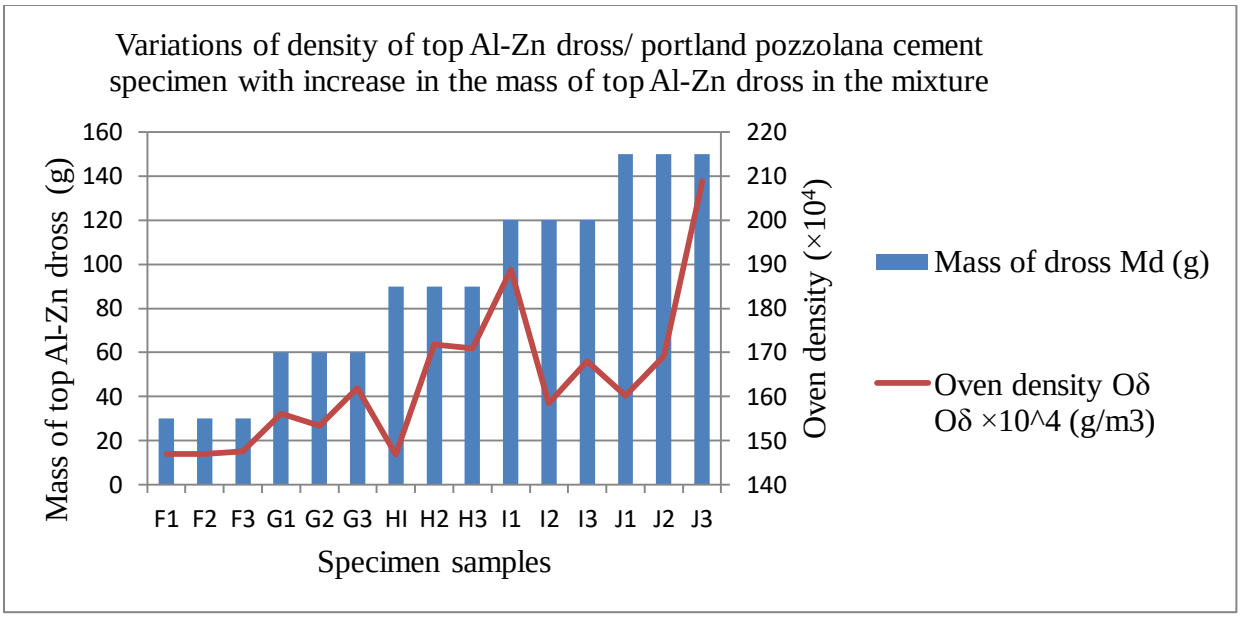

FIG. 4- 3 Variation of the density with changes in the mass of top Al-Zn dross in the specimen

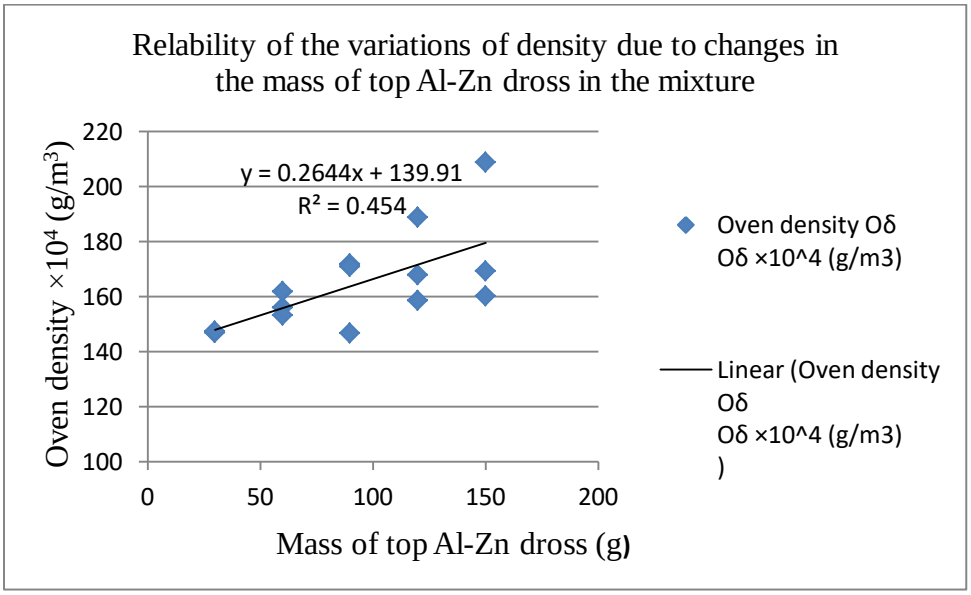

FIG. 4- 4 Reliability of changes in density with an increase in the mass of top Al-Zn dross

4.4 Variation of Porosity of the Top Al-Zn Dross/ Portland Pozzolana cement specimen with an increase in the mass of Top Al-Zn dross

TABLE 4- 5 Summary of results from Appendix 3.1

Mass of top Al-Zn dross Md (g)	**Top Al-Zn dross/ Portland pozzolana cement slab**	**Calculated porosity Vr (%)**
30	F1	14.9
	F2	17.4
	F3	19.6
60	G1	19.7
	G2	18.5
	G3	16.3
90	H1	22.3
	H2	15.1
	H3	18.5
120	I1	23.6
	I2	21.7
	I3	26
150	JI	33
	J2	33.3
	J3	21

From the graph in FIG. 4-5, an increase in the mass of dross in the top Al-Zn dross/ portland pozzolana cement slab increases porosity. The increase in porosity is due to the increased evolution of hydrogen gas as a result of the increased reactive chemical activity.

FIG. 4-6 shows that 56.83% of the increase is porosity is due to the increase in the mass of top Al-Zn dross in the top Al-Zn dross/ portland pozzolana cement specimen, indicated by the

coefficient of determination R^2 =0.5683. A positive gradient confirms that increase in the mass of top Al-Zn dross increases the porosity of the specimen.

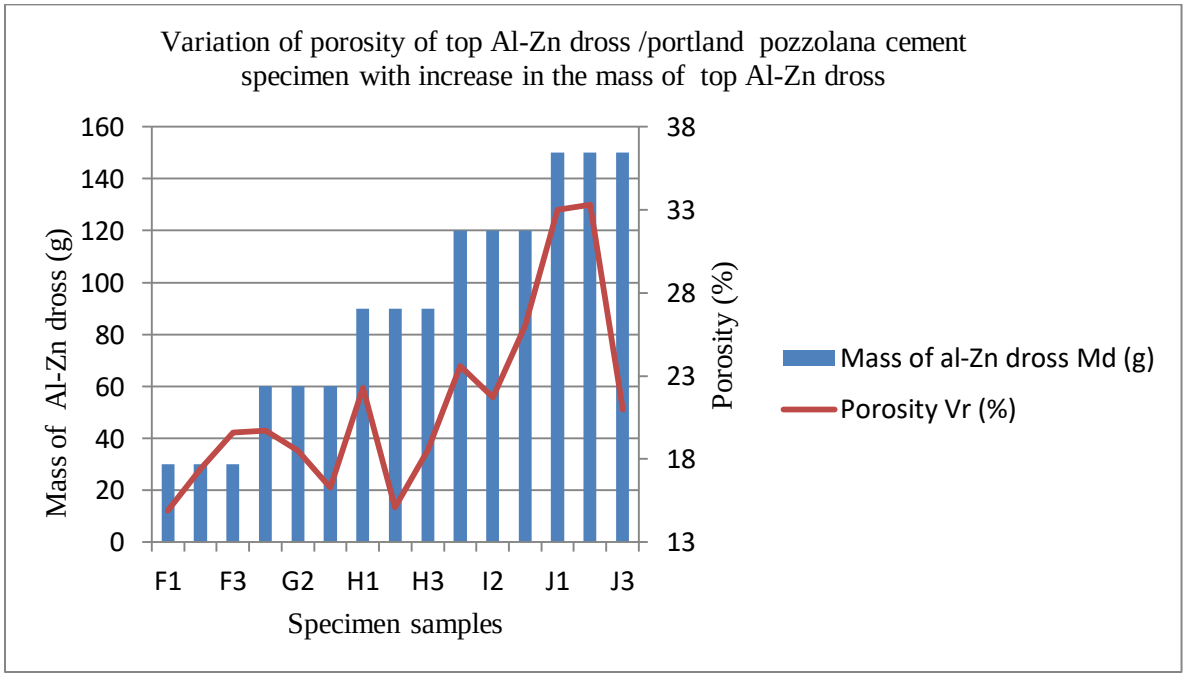

FIG. 4- 5 Variation of the porosity with changes in the mass of top Al-Zn dross in the specimen

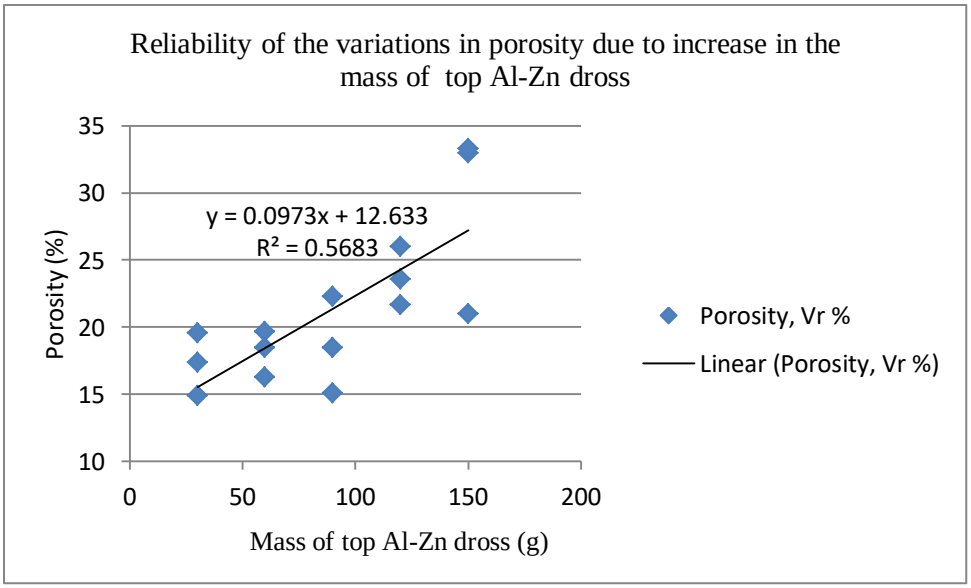

FIG. 4- 6 Reliability of the changes in porosity with an increase in the mass of top Al-Zn dross

4.5 Variation of Permeability of the Top Al-Zn Dross/ Portland Pozzolana Cement Specimen with an Increase in the Percentage Mass of Top Al-Zn Dross.

TABLE 4- 6 Summary of the results from Appendix 4.1

% mass of top Al-Zn dross in the sample %	Top Al-Zn dross/ portland pozzolana cement slab	Permeability coefficient K (mm/s)
10	W1	0
	W2	0
	W3	0
20	VI	0.0018
	V2	0.0010
	V3	0.0022
30	U1	0.0222
	U2	0.0043
	U3	0.0060
40	T1	0.0040
	T2	0.0043
	T3	0.0023
50	S1	0.0022
	S2	0.0021
	S3	0.0066

The dross specimen samples T1, T2, T3, S1, S2, and S3 were softened when soaked in water and were easily eroded by rubbing with hands. Two specimens' samples, T1 and S2 developed cracks separating into half after conducting the permeability tests (Fig 4.7). The cracks were caused by the compressive forces along the height L3 of the cast specimen during the process conducted to ensure a watertight seal during the permeability test furthermore, the cracks may

have been caused by the process of forcing out the specimen samples from the permeability test equipment.

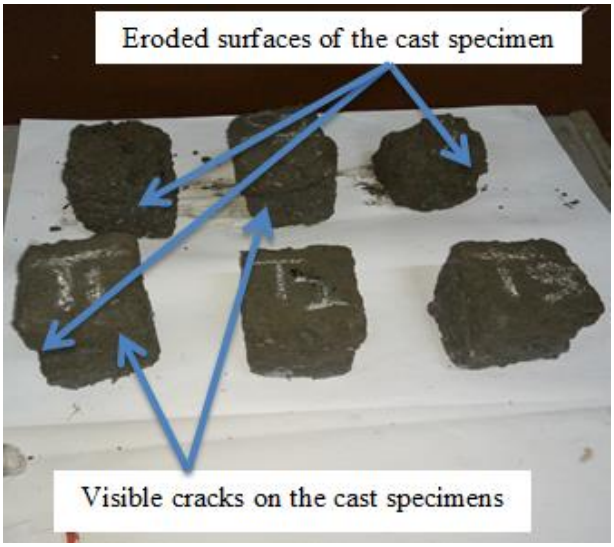

FIG. 4- 7 Soaked specimens from concrete design F and G

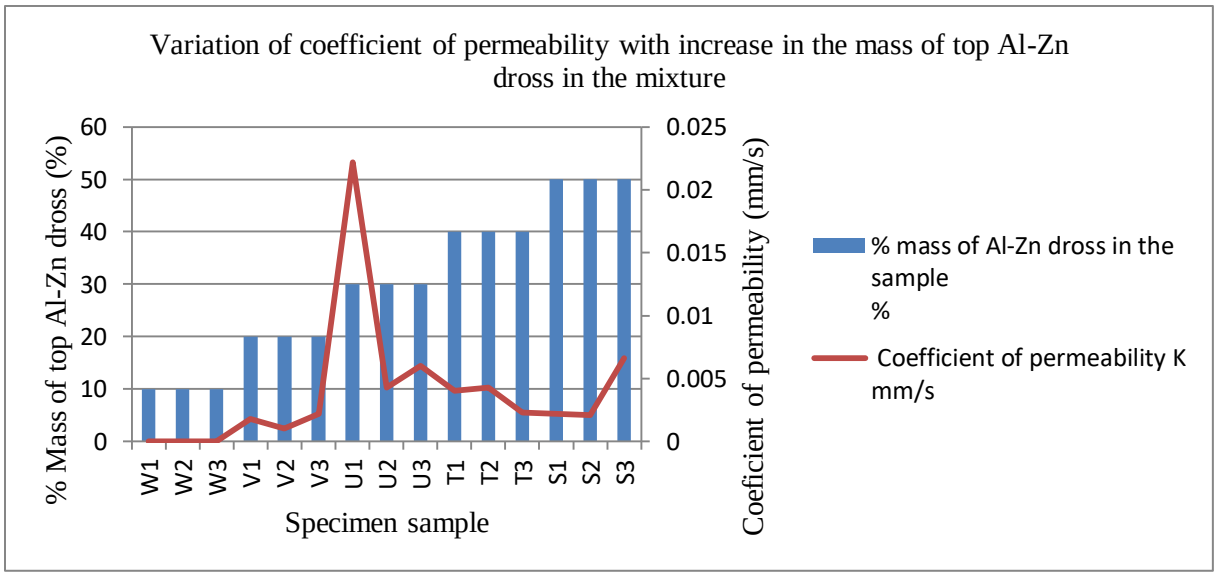

FIG. 4- 8 Variation of the coefficient of permeability with changes in the mass of Top Al-Zn dross

An increase in the percentage mass of top Al-Zn dross in the mixture gradually increased the permeability coefficient of the top Al-Zn dross/ portland pozzolana cement slab. At low % mass

concentrations of 10%, there was no water seepage through the slab. Seepage was recorded in slabs containing 20 % mass of top Al-Zn dross which gradually increased with an increase in the percentage mass of top Al-Zn dross due to the increased chemical activity accompanied by increased evolution of hydrogen gas.

FIG. 4-9 shows the relationship between the variation in permeability of the concrete slabs and the mass percentage of top Al-Zn dross in the specimen samples. The low coefficient of reliability R^2 = 0.06 is an indication that not all pores created in the top Al-Zn dross/ portland pozzolana cement specimen allow the flow of water through it.

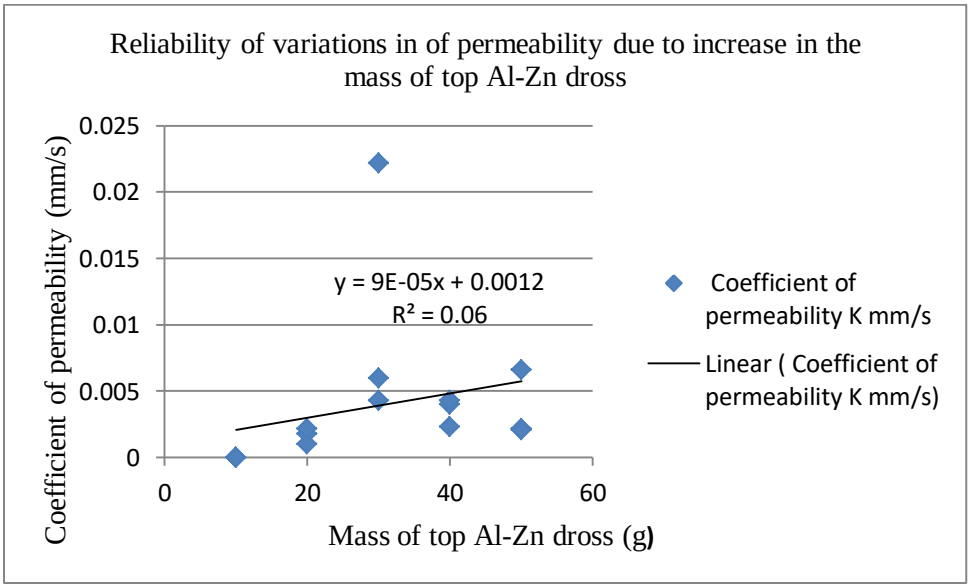

FIG. 4- 9 Reliability of the changes permeability with an increase in the mass of top Al-Zn dross

4.6 Variation of Compressional Strength with Mass of Top Al-Zn Dross

TABLE 4- 7 Summary of results from Appendix 5.1

% mass of top Al-Zn dross in the sample (%)	Top Al-Zn dross/ portland pozzolana cement slab	Compressional strength Cs × 10^{-3} (N/mm2)
10	W1	8.0974
	W2	8.8065
	W3	9.4296
20	V1	8.4112
	V2	9.8246
	V1	6.7215
30	U1	5.643
	U2	7.1562
	U3	8.6496

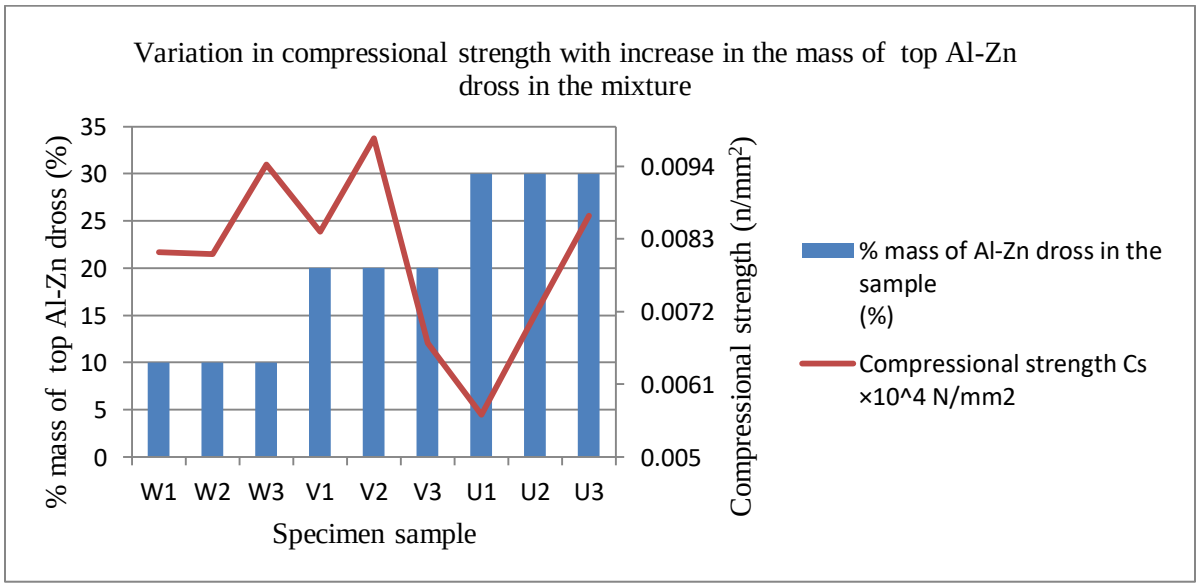

FIG. 4- 10 Variation of compressional strength with changes in the mass of top Al-Zn dross

Al-Zn dross/ portland pozzolana cement specimens S1, S2, S3, T1, T2, and T3 were not subjected to compressional test because they had developed cracks, which would generate unreliable results.

FIG. 4-10 shows that an increase in the percentage mass of Al-Zn dross caused a decrease in the compressional strength of slabs. The observed trend is due to the increase in porosity of the Al-Zn/cement slabs which reduces the structural integrity of the Al-Zn Dross/ Portland pozzolana cement slab, therefore, weakening it.

The coefficient of reliability R^2 = 0.2061 in Fig. 4-11 is an indication that 20.61 % of the variations in the compressional strength is as a result of the changes mass of Al-Zn dross. A negative gradient indicates that the increase in the % mass of Al-Zn dross reduces the compressional strength.

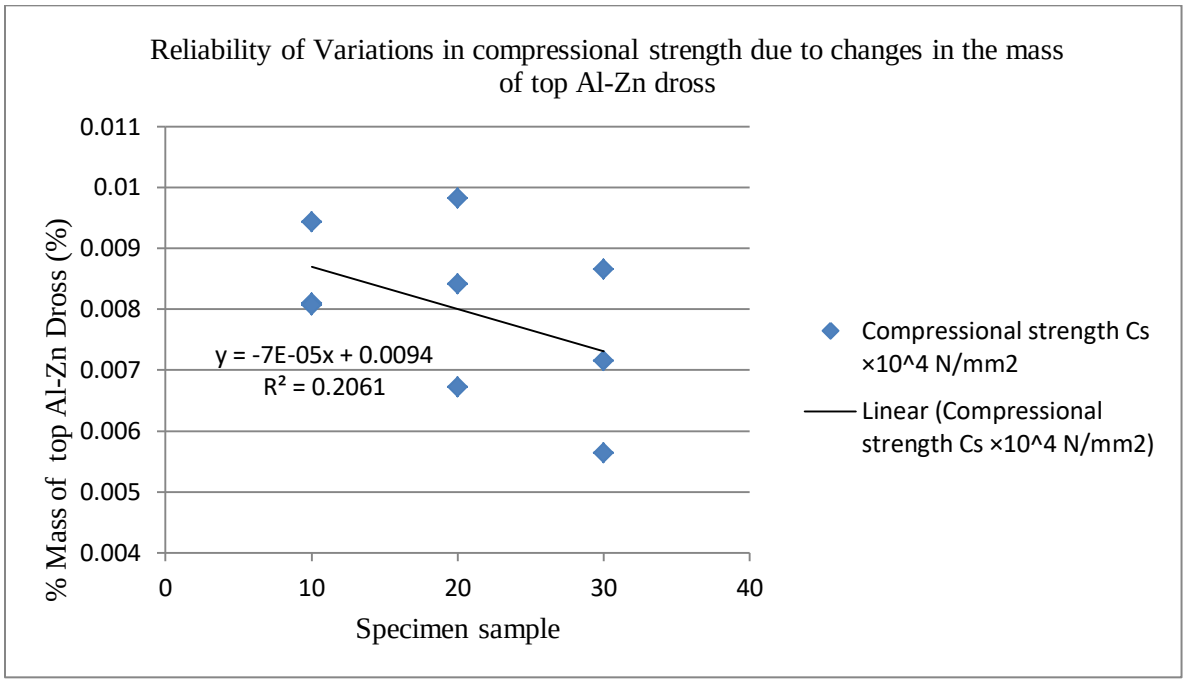

FIG. 4- 11 Reliability of the changes in porosity with an increase in the mass of top Al-Zn dross

4.7 The Optimum % Mass of Top Al-Zn Dross in the Top Al-Zn Dross/ Portland Pozzolana Cement Mixture

An extract of results from the experiment used to determine the coefficient of permeability and compressional strength was used to determine the optimum percentage mass of top Al-Zn dross that can be added in top Al-Zn dross/ Portland pozzolana cement mixture to produce slabs with a maximum coefficient of permeability and compressional strength.

TABLE 4- 8 Results for optimization of compressional strength and coefficient of permeability

% mass of top Al-Zn dross in the sample (%)	**Permeability, K (mm/s)**	**Compressional strength Cs $\times 10^{-3}$ (N/mm^2)**
10	0	8.0974
10	0	8.8065
10	0	9.4296
20	0.0018	8.4112
20	0.0010	9.8246
20	0.0022	6.7215
30	0.0222	5.643
30	0.0043	7.1562
30	0.0060	8.6496

From the graph annexed in appendix 6-1, an increase in the coefficient of permeability results in a reduction in the compressional strength of the top Al-Zn dross/ Portland pozzolana cement specimen. The mass percentage of top Al-Zn dross in the range of 39% can be used to produce slabs with a combination of maximum coefficient of permeability and maximum compressional strength.

CHAPTER FIVE

5.0 CONCLUSIONS AND RECOMMENDATION

5.1 Conclusions

Top Al-Zn dross from Roofings Rolling Mills Ltd galvanizing bath is made up of many elements with aluminium and zinc having the greatest percentage occurrences. The average percentage occurrences of aluminium and zinc in top Al-Zn dross is further indicated by comparison with the microstructure of Al-Zn alloys. The large percentages of aluminium and zinc are explained by two factors namely; they are the chief coating materials that are added into the galvanizing bath and, the metallic Al and Zn are scooped together with top Al-Zn dross. The percentage occurrence of aluminium and zinc in top Al-Zn dross correlates with the percentage of aluminium and zinc added during the charging process of the galvanizing bath. The numerous elements found in top Al-Zn dross coupled with the favorable high-temperature conditions favor chemical reactions to form various compounds. The various compounds formed are randomly distributed across the surface of the top Al-Zn dross and are responsible for the varying hardness values.

Top Al-Zn dross contains reactive aluminium which reacts when mixed with portland pozzolana cement and water, in an exothermic reaction with the evolution of hydrogen gas. The rate of evolution of the hydrogen gas is dependent on the quantity of top Al-Zn dross added into the mixture, therefore, top Al-Zn dross from RMM Ltd can be used as a foaming agent when mixed with portland pozzolana cement to produce porous concrete block. The addition of top Al-Zn dross in portland pozzolana cement causes an increase in density and porosity in top Al-Zn dross/ portland pozzolana cement mixture, with the rate of increase in the variables related to the mass percentage of top Al-Zn dross added. Permeability is only induced when the mass percentage of top Al-Zn dross in the mixture is above 10%, which implies that pores responsible for permeability are caused by vigorous chemical reactions capable of creating wider and longer open pores between two-dimensional surfaces of the top Al-Zn dross/ Portland pozzolana cement slabs. Compressional strength is reduced with the addition of top Al-Zn dross due to the reduction in the structural integrity of the cast top Al-Zn dross/ portland pozzolana cement slabs. A mixture containing 39% of top Al-Zn dross produces top Al-Zn dross/ portland pozzolana

cement slabs with a combination of maximum coefficient of permeability and maximum compressional strength.

The implementation of the project will introduce two products in the market, porous and permeable slabs which can be used in water seepage applications and porous and impermeable blocks which have excellent applications in thermal and noise insulations in construction industry. The products will be marketable since they can be locally utilized. The use of top Al-Zn dross in the development of porous and impermeable blocks for construction purposes will reduce, at most prevent the dispersion of toxic materials into the environment.

5.2 Recommendations

Further research needs to be conducted to develop top Al-Zn dross/ portland pozzolana cement slabs using uniformed size top Al-Zn dross particles. The top Al-Zn dross/ portland pozzolana cement slabs could be developed with the addition of other wastes like broken bricks, tiles, etc. The reaction of top Al-Zn dross with other types of cement from different manufacturers should be investigated to determine their characteristic behavior.

The water filtered through the top Al-Zn dross/ cement slabs should be analyzed to determine the presence and the level of toxicity in them so as to access its environmental impact. The economic analysis needs to be carried out to determine the viability of the project

REFERENCES

1. Agatzini-Leonardou, S., Zafiratos, I., & Oustadakis, P. (2000.). Patent No. Greek Patent GR1003419. Greece.
2. Ainsley Mike (2012 March). Technical Seminar for Galvanizers, International Zinc Association. Improving the Productivity and Quality in Hot Dip Galvanization Process. Retrieved August 8, 2018, from www.coezinc.com.
3. Alane, N., Djerad, S., & Tifouti, L. (2008). "Acid Leaching of Zinc Oxide from ZnO/Al2O3 Catalyst. Lebanese Science Journal, Vol. 9, No. 2.
4. American Society for Metals. (1972). Atlas of Microstructure of Industrial Alloys. In M. P. ASM, Metals Handbook, 8th ed. Vol. 7. OH: American Society of Metals. Metals Hand Book, 8th ed, Vol.7
5. ASTM International (2000). ASTM C 567-00: Standard test for determining Density of Structural Light Weight Concrete. Retrieved June 10, 2018, from http://www.c-s-h.ir/wp-content/uploads/2014/12/C-567.pdf
6. ASTM International. (2011). ASTME 18-11: Standard Test Methods for Rockwell Hardness of Metallic Materials. Retrieved June 8, 2018, from https://www.scribd.com/document/348011852/E18-11-pdf
7. Avik Mondal, Arup Kumar Halder, Soumilya Nayak, Amrendra Kumar, Anidita Chakraborty, Shweta Shukla, Sibasis Sahoo, Rajesh S. Pais, Monojit Dutta, "Root cause analysis on uncommon surface defects on the galvannealed steel sheet", Engineering Failure Analysis, vol 93, November 2018, pp. 66-75
8. Barakat, M. A. (2009). Pyrometallurgical processing of Dross. The Open Mineral Processing Journal, Vol. 2, 12-16.
9. Barakat. (2003). The Pyrometallurgical Processing of Galvanized Zinc Ash and Flue Dust. Journal of Metals, TMS, 26-29.
10. Barber. (1972). PFA Utilization London. Central Electricity Generation Board.
11. BSI. (1983). BS 1881-116: Method for determination of compressive strength of concrete cubes: Retrieved July 11, 2018, from https://standards.globalspec.com/std/780230/bsi-bs-1881-116

12. Cook, D. (1997). Saw Dust, Ash, Lime, Cement Mixes for use in Masonry Units. Building and Environment, 218-220.
13. Çoupur, M., Özmetin, C., Özmetin, E., & Kocakerim, M. (2004). Optimization Study of the Leaching of Roasted Zinc Sulphide Concentrates with Sulphuric Acid Solutions. Chemical Engineering and Processing: Process Intensification, 43(8), 1007-1014.
14. D. Horstmann, Faults in the hot dip galvanizing plant. Stahleisen M.b H., Dusseldorf (1975)
15. Da¨rr, G., & Ludwing, U. (1973). Determination of Permeable Porosity. Mater. Struct. 6 (2), 185– 90.
16. De-Wet, J. R., & Singleton, J. D. (2008). Development of a viable process for the recovery of zinc from oxide ores. Journal of the South African Institute of Mining and Metallurgy, 108(5), 253-259.
17. Dong, A., Shu, J., Wang, J., Cai, X., Sun, B., Cui, J., et al. (2008). Continuous Separation of Fe-Al-Zn Dross from Hot Galvanized Melt using Alternating Magnetic Field. Mater. Sci. Techno. 24, 40-44.
18. DuBois, M., "Top drosses: the undocumented gold mine", Galvanizer's Association Annual Meeting, 2003, Monterrey, Mexico
19. Elżbieta, R.-L., Mariusz, S., & Włodzimierz, U. (2015). Recovery of Zinc from Metallurgic Waste Sludges. Pol. J. Environ. Stud. Vol. 24, No. 3, 1277-1282.
20. Everitt, M. (2006). Profitable Recycling of Galvanized Scrap. 11th International Galvanizing and Coil Coating Conference. Metal Bulletin.
21. Fajardo, O., Henao, S., & Baines, D. (2014). Crystal Structure of Aluminum, Zinc, and Their Alloys. ENGR45, SRJC: Retrieved July 27, 2018 from http://www.santarosa.edu/~yataiiya/E45/PROJECTS/MicroStructure%20of%20Aluminum,%20Zinc.pdf
22. Goodhew, P. J. (April 1973). Specimen Preparation in Material Science, in Practical Methods in Electron Microscopy. New Holland, New York: Elsevier Science Publishing Co. Inc., U.S.

23. Halloway, P. C., Etsell, T., & Murland, A. (2007). Use of Secondary Additives to Control Dissolution of Iron during Na_2CO_3 Roasting Metal. Mater.Trans. B 39, 793-808.
24. Hegewaldt, F. (2001, May 17- 18.). Recycling of zinc Coated Steel Sheets. Modeling for Saving Resources, International Scientific Colloquium, pp. 164-168.
25. Holt, E., & Raivio, P. (2005). Use of Gasification Residues Aerated Autoclaved Concrete Cement. Cement and Concrete Research 35, 796-802.
26. I.G Murgulescu, O. Radovici, M. Borda, 1965. Studies on the Mechanism of Anodic Dissolution of Al-Zn Binary Alloys in Alkaline Solutions by Potentiodynamic and Potentiostatic Pulse method. Corros. Sci. 5, 613-623
27. Ilinca, F., Ajersch, F., Baril, C., & Goodwin, F. E. (2007). Numerical Simulation of the Galvanizing Process during GA to GI transition. Int. J. Meth. Fluids; 53, 1629-1646.
28. Kozlowski, J., & Laskawiec, J. (2000). Intermetallics, Vol. 8, No.12, 1439-1442.
29. Kreibich, V. (2007). Problematika předúprav povrchu. Povrchová úprava. Retrieved March 17, 2018, from http://www.povrchovauprava.cz/uploads/assets/ casopisy/pu 2007-03.pdf
30. Leclerc, N., meux, E., & Lecuire, J.-M. (2002). Hydrometallurgical Recovery of Zinc and Lead from Electric Arc Furnace Dust using Mononitrilotriacetate Anion and Hexahydrated Ferric Chloride. Journal of Hazardous Materials, B91, 257-270.
31. Liberski, P. (2008). Theoretical and Practical Aspects of Zinc Coatings on Ferroalloys Created by Hot Dip Galvanizing Process. Conference zaroveho zinkovani (pp. 42-51). Hrotovice: ISBN 978-80-254-2679-1.
32. Liu, X. B., & Lin, H. C. (2010). Analyses of Zinc Pot Roller Slagging at Galvanized. Metal World, 2, 37–39.
33. Liu, Y., Tang, N., Zhang, L., Denner, S., & Goodwin, F. (2002). Dross Formation and Control during Transition from Galvannealing to Galvanizing. 44th MWSP Conference Proceeding (pp. 781–790). Iron & Steel Society.
34. Luo, Q., Jin, f., Li, Q., Jie-Yu, C., & Kuo-Chih. (2013). The Mechanism of Dross Formation during Hot Dip Al-Zn Alloy Coating Process. Journal for Manufacturing Science and Production. VL. 13, 10.1515L/ jmsp-2012-0023.

35. M. Gagne, A. Pare, F. Ajersch, “Water Modelling of a Continuous Galvanizing Bath” 84th Galvanizers Association Meeting Proceedings, October 1992, pp.147-163
36. Maass, P., & Peissker, P. (2011.). Handbook of Hot-dip Galvanization. WILLEY-VCH.
37. Mahbubur, R., Raibul Qadir, M., Tahuran Neger, A., & Kurny, A. (2013). Studies on the Preparation of Zinc Oxide from Galvanizing plant. American Journal of Material Engineering and Technology, Vol. 1, No. 4, 59-64.
38. Marder, A. (2000). The Metallurgy of Zinc-Coated Steel. Progress in Materials Science, 45, 191-271.
39. Mark A. Bright, Nathan J. Deem, John Fryatt, 2007. “The advantages of recycling metallic zinc from the processing wastes of industrial molten zinc applications”. The Minerals, Metals & Materials Society.Metallics Systems a division of Pyrotek Inc. 31935 Aurora Road Solon, Ohio email: marbri@pyrotek-inc.com
40. Martin, D., Regife, J., & Nogueria, E. (1983). Patent No. Pat. 4401531. US.
41. McCall, J. L., & William, M. M. (1974). Metallographic Specimen Preparation for Optical and Electron Microscopy. New York: Plenum Press.
42. Miao, H. L. (2005). The Control of Bottom Slag in Band Steel Galvanizing. Hunan Nonferrous Metals, 21 (1), 30–61.
43. MIN Xiao-bo, Xian-de, X., Li-yuan, C., Yan-jie, L., Mi, L., & Yong, K. (2013). Environmental Availability and Ecological Risk Assessment of Heavy Metals in Zinc Leaching Residue. Transactions of Nonferrous Metals Society of China, 23 (1), 208−218.
44. Mobasher, B. (2011). Mechanics of Fibre and Textile Reinforced Cement Composites. Boca Raton, fla.: London: Boca Raton, Fla: CRC.
45. Nagraj, T., & Zahida, B. (1996). Generalization of Abrams’ laws. Cem. Concr. Res. 26 (6), 933– 942.
46. Nakano, J., Purdy, G., & Malakhov, D. (2002). Modeling of Intermetallic Formation in Hot-Dip Galvanizing. XXXI CALPHAD Meeting Proceedings.
47. Nooman, M. T. (2016). Effect of Zeolite Inclusion on Some Properties of Concrete and Corrosion Rate of Reinforcing Steel Bars Embedded in Concrete. IOSR Journal

of Mechanical and Civil Engineering (IOSR-JMCE) e-ISSN: 2278-1684,p-ISSN: 2320-334X, Volume 13. Issue 6, Ver.1, 51-59.

48. N-Y. Tang. (2000). Determination of Liquid Phase Boundaries in the Zn-Fe-Mx System. Journal of Phase Equilibria, Vol. 21, No.1, 70-77.
49. O'Dell, S., Charles, J., Vlot, M., & Randle, V. (2004). Modeling of Iron Dissolution during Hot Dip Galvanizing of Strip Steel. Materials Science and Technology, 20:2, 251-256.
50. Özverdi, A., & Erdem, M. (2010). Environmental Risk Assessment and Stabilization/Solidification of Zinc Extraction Residue. Environmental risk assessment [J].Hydrometallurgy, 100(3−4), 103−109.
51. Puertas, F., Blanco-Verela, M., & Vazuez, T. (1999). The Behavior of Cement Mortars containing Industrial Waste from Aluminium Refining Stability In Ca(OH) solutions. Cement and Concrete research. Vol. 29, 1673-1680..
52. Rabah, M. A., & El-Sayed, A. (1995). Recovery of Zinc and some of its Valuable Salts from Secondary Resources and Wastes. Hydrometallurgy 37, 23-32.
53. Rakesh, K., & Bhattacharjeeb, B. (2003). Porosity, Pore Size Distribution and in Situ Strength of Concrete. Cement and Concrete Research 33, 155–164.
54. Rama Mahalingam, Shanthi Vaithiyalingam Mahalingam. (2016). Analysis of Pervious Concrete Properties. GRADEVINAR 686, 493-501.
55. Reinhardt, H., Aguado, A., Gettu, R., & Shah, S. (. (1995). Concrete Technology. New Trends Industrial Applications E & FN Spon, UK, 19–32.
56. Roofings Rolling Mills Ltd. (2013). *Roofings Group.* Retrieved March 20, 2018, from Roofings Rolling Mills Ltd: http://www.roofingsgroup.com/index.php?option=com_content&view=article&id=49:roofing-rolling-mills&catid=34:content-demo.
57. Rostasy, F., Weib, R., & Wiedemann, G. (1980). Changes of Pore Structure of Cement Mortar due to Temperature. Cem. Concr. Res. 10 (2), 157– 164.
58. Schiller, K. (1971). The strength of Porous Materials. Cement and Concrete Research. 1 (4), 419–422.

59. Shawki, S., & Hamid, Z. A. (2003). Effect of Aluminium Content on the Coating Structure and Dross Formation in the Hot-Dip Galvanizing Process. Surface and Interface Analysis, 35, 943–947.
60. Silva, J. E., D, S., Paiva, A., Labrincha, J., & Castro, F. (2005). Leaching Behavior of Galvanic Sludge in Sulphuric Acid and Ammoniacal Media. Journal of Hazardous Materials, B 121, 195-202.
61. Sulaiman, S.H. (2011). "Water Permeability and Carbonation on Foamed Concrete," M.S. thesis, University of Tun Hussein Onn Malaysia.
62. Tracz, T. (2016). Open Porosity of Cement Pastes and their Gas Permeability. Bulletin Of The Polish Academy Of Sciences Technical Sciences, Vol. 64, No. 4, DOI: 10.1515/bpasts-2016-0086.
63. Trpcevská, J., Hluchánová, B., Vindt, T., Zorawski, W., & Jakubéczyová, D. (2010). Characterization of the Bottom Dross Formed during Batch Hot-Dip Galvanizing and it's Refining. Acta Metallurgica Slovaca, Vol. 16, No.3, 151-156.
64. Turan, D., Altundogan, S., & Tqmen, F. (2004). Recovery of Zinc and Lead from Zinc Plant Residue. Hydrometallurgy 75, 169-176.
65. Uganda Bureau of Statistics. (2018). Performance of the Ugandan Economy for Fiscal Year 2016/2017. Retrieved November 21, 2018, from Uganda Bureau of Statistics: https://www.ubos.org>uploads>ubos
66. VanderVoort, G. F. (1984). Metallography- Principles and Practice. ASM International- McGraw-Hill. New York.
67. Varadarajan, A. (2008). Dross Formation Mechanism and Development of Wear Resistant Scrapper in 55 Al- 1.5 Si- Zn Coating Bath, Ph.D. Dissertation. West Virginia University.
68. Vikas, S., Agarwal, V., & Rakesh, K. (2012). Effect of Silica Fume on Mechanical Properties of Concrete". Acad. Indus. Res. Vol. 1 (4), 176-179.
69. Vipin, H., Monali, I., Ganesh, W., Girish, S., Poonam, I., & Amit, K. (2017, June). Effect of Fly Ash and Polymer on Compressive Strength of Concrete. The International Research Journal of Engineering and Technology (IRJET) e-ISSN: 2395 -0056 Volume: 04 Issue: 06: Retrieved August 15, 2018, from https:/www.irjet.net/archives/V4/i6/IRJET-V41676.pdf

70. Vourlias, G., Pistofidis, N., Pavlidou, E. S., & Polychroniadis, E. (2007). Journal of Optoelectronics and Advanced Materials, Vol. 9, No. 9, 2937-2942.
71. Willis, D. (2005). Development of Hot dipped Metallic-Coated Steel processing. Materials Forum, 29 (1), 9-16.
72. Winslow, D., & Liu, D. (1990). Pore Structure of Paste in Concrete. Cem. Concr. Res. 20 (2), 227-235.
73. Yen, L. (2006). M.S. thesis, Study of Water Ingress into Foamed Concrete. The National University of Singapore.
74. Zhen-guang, R., Cen-xuan, P., Gui-hua, L., Xue-ting, W., Guang-yu, D., & Ke-song, Z. (2015). Leaching and Recovery of Zinc From Leaching Residue of Zinc Calcine Based on Membrane Filter Press. Trans. Nonferrous Met. Soc. China 25, 622−627.

APPENDICIES

Appendix 1.1: Specimen A- Chemical Composition

SPECTRO

Sample Results

Sample Result Name	Type	Measure Date Time	Recalculation Date Time	Origin
TOP DROSS/BETTY	Unknown	17/08/2018 11:29	17/08/2018 11:32	Measured

Method Name	Check Type	Check Status	Correction Type	Outlier Test Type
Zn-80-M	None	Not Used	None	None

Status
Not Used

Sample Name	Analyst	Shift
TOP DROSS	BETTY	A

	Al Conc %	Cu Conc %	Pb Conc %	Sn Conc %	Cd Conc %	Fe Conc %	Mg Conc %	Mn Conc %	Si Conc %	Zn Conc %
1	54.4	<0.100	0.003	A 0.006!	0.0003	>0.14	0.003	A 0.003!	A 1.40!	43.99
2	52.3	<0.100	0.003	A 0.007!	0.0004	>0.14	0.004	A 0.006!	A 1.38!	46.08
3	54.0	<0.100	0.002	A 0.007!	0.0005	>0.14	0.004	A 0.006!	A 1.35!	44.39
Min Cal	10.00	0.100	0.0004	0.0005	0.0002	0.0004	0.0005	0.0005	0.0001	--
Rep	53.5	<0.100	0.003	A 0.007!	0.0004	>0.14	0.004	A 0.005!	A 1.38!	44.82
Max Cal	60.0	3.20	0.010	0.015	0.009	0.14	0.060	0.009	2.70	--
Mean	53.5	<0.057	0.003	A 0.007!	0.0004	>8.31	0.004	A 0.005!	A 1.38!	36.69
SD	1.11	0.0000	0.0001	0.0004	0.0001	0.0000	0.0004	0.001	0.026	2.22
RSD	2.07	0.0000	2.46	6.52	25.12	0.0000	11.08	28.86	1.87	4.95

Appendix 1.2 Specimen B- Chemical composition

SPECTRO

Sample Results

Sample Result Name	Type	Measure Date Time	Recalculation Date Time	Origin
TOP DROSS/BETTY	Unknown	14/08/2018 12:24	14/08/2018 12:28	Measured

Method Name	Check Type	Check Status	Correction Type	Outlier Test Type
Zn-80-M	None	Not Used	None	None

Status
Not Used

Sample Name	Analyst	Shift
TOP DROSS	BETTY	A

	Al Conc %	Cu Conc %	Pb Conc %	Sn Conc %	Cd Conc %	Fe Conc %	Mg Conc %	Mn Conc %	Si Conc %	Zn Conc %
1	A 36.31!	A 0.57!	A 0.008!	A 0.015!	A 0.008!	A 0.14!	A 0.015!	A 0.009!	A 1.47!	61.5
2	A 37.13!	A 0.21!	A 0.007!	A 0.015!	A 0.002!	A 0.14!	A 0.014!	A 0.007!	A 1.50!	61.0
3	A 46.47!	A 0.12!	A 0.004!	A 0.006!	0.0007	A 0.14!	A 0.012!	A 0.005!	A 1.66!	51.6
Min Cal	**10.00**	**0.100**	**0.0004**	**0.0005**	**0.0002**	**0.0004**	**0.0005**	**0.0005**	**0.0001**	--
Rep	A 39.97!	A 0.30!	A 0.006!	A 0.012!	A 0.003!	A 0.14!	A 0.014!	A 0.007!	A 1.54!	***58.0***
Max Cal	**60.0**	**3.20**	**0.010**	**0.015**	**0.009**	**0.14**	**0.060**	**0.009**	**2.70**	--
Mean	A 39.97!	A 0.30!	A 0.006!	A 0.18!	A 0.003!	A 3.03!	A 0.014!	A 0.008!	A 1.54!	**54.9**
SD	***5.64***	***0.24***	***0.002***	***0.005***	***0.004***	***0.0000***	***0.001***	***0.002***	***0.10***	***9.00***
RSD	***14.12***	***78.6***	***30.23***	***41.85***	***111***	***0.0000***	***10.50***	***29.38***	***6.75***	***15.51***

Appendix 1.3 Specimen C- Chemical composition

SPECTRO

Sample Results

Sample Result Name	Type	Measure Date Time	Recalculation Date Time	Origin
TOP DROSS "C"/BETTY	Unknown	31/08/2018 11:54	31/08/2018 11:56	Measured

Method Name	Check Type	Check Status	Correction Type	Outlier Test Type
Zn-80-M	None	Not Used	None	None

Status
Not Used

Sample Name	Analyst	Shift
TOP DROSS "C"	BETTY	A

	Al Conc %	Cu Conc %	Pb Conc %	Sn Conc %	Cd Conc %	Fe Conc %	Mg Conc %	Mn Conc %	Si Conc %	Zn Conc %
1	53.8	<0.100	0.002	A 0.005!	0.0002	>0.14	0.002	A 0.003!	A 1.24!	44.75
2	53.8	<0.100	0.003	A 0.006!	0.0003	>0.14	0.003	A 0.002!	A 1.56!	44.41
3	55.6	<0.100	0.002	0.005	<0.0002	>0.14	0.002	A 0.001!	A 1.21!	42.97
Min Cal	10.00	0.100	0.0004	0.0005	0.0002	0.0004	0.0005	0.0005	0.0001	--
Rep	*54.4*	<0.100	*0.003*	A 0.005!	*0.0002*	>0.14	*0.003*	A 0.002!	A 1.34!	*44.04*
Max Cal	60.0	3.20	0.010	0.015	0.009	0.14	0.060	0.009	2.70	--
Mean	54.4	<0.053	0.003	A 0.005!	0.0002	>2.17	0.003	A 0.002!	A 1.34!	42.06
SD	*1.04*	*0.0000*	*0.0002*	*0.0006*	*0.0000*	*0.0000*	*0.0006*	*0.0008*	*0.19*	*0.44*
RSD	*1.91*	*0.0000*	*6.33*	*10.38*	*16.76*	*0.0000*	*24.47*	*43.90*	*14.22*	*1.01*

Appendix 1.4 Specimen D- Chemical composition

SPECTRO

Sample Results

Sample Result Name	Type	Measure Date Time	Recalculation Date Time	Origin
TOP DROSS "D"/BETTY	Unknown	31/08/2018 12:03	31/08/2018 12:05	Measured

Method Name	Check Type	Check Status	Correction Type	Outlier Test Type
Zn-80-M	None	Not Used	None	None

Status
Not Used

Sample Name	Analyst	Shift
TOP DROSS "D"	BETTY	A

	Al Conc %	Cu Conc %	Pb Conc %	Sn Conc %	Cd Conc %	Fe Conc %	Mg Conc %	Mn Conc %	Si Conc %	Zn Conc %
1	49.63	<0.100	0.003	A 0.007!	0.0004	>0.14	0.004	A 0.006!	A 1.37!	48.75
2	55.4	<0.100	0.002	A 0.006!	0.0003	>0.14	0.003	A 0.003!	A 1.38!	42.92
3	53.3	<0.100	0.002	A 0.006!	0.0004	>0.14	0.003	A 0.005!	A 1.33!	45.13
Min Cal	10.00	0.100	0.0004	0.0005	0.0002	0.0004	0.0005	0.0005	0.0001	--
Rep	*52.8*	<0.100	*0.002*	A 0.006!	*0.0004*	>0.14	*0.003*	A 0.005!	A 1.36!	*45.60*
Max Cal	60.0	3.20	0.010	0.015	0.009	0.14	0.060	0.009	2.70	--
Mean	52.8	<0.052	0.002	A 0.006!	0.0004	>8.03	0.003	A 0.005!	A 1.36!	37.76
SD	*2.94*	*0.0000*	*0.0001*	*0.0006*	*0.0001*	*0.0000*	*0.0006*	*0.001*	*0.029*	*1.26*
RSD	*5.57*	*0.0000*	*6.04*	*9.50*	*23.76*	*0.0000*	*16.89*	*28.22*	*2.13*	*2.77*

Appendix 1.5: Specimen E- Chemical composition

SPECTRO

Sample Results

Sample Result Name	Type	Measure Date Time	Recalculation Date Time	Origin
TOP DROSS "E"/BETTY	Unknown	31/08/2018 12:11	31/08/2018 12:14	Measured

Method Name	Check Type	Check Status	Correction Type	Outlier Test Type
Zn-80-M	None	Not Used	None	None

Status
Not Used

Sample Name	Analyst	Shift
TOP DROSS "E"	BETTY	A

	Al Conc %	Cu Conc %	Pb Conc %	Sn Conc %	Cd Conc %	Fe Conc %	Mg Conc %	Mn Conc %	Si Conc %	Zn Conc %
1	A 47.41!	<0.100	A 0.006!	A 0.008!	0.0008	A 0.14!	A 0.012!	A 0.007!	A 1.72!	50.6
2	46.10	<0.100	A 0.003!	A 0.008!	0.0007	A 0.14!	A 0.010!	A 0.008!	A 1.37!	52.3
3	42.00	<0.100	A 0.003!	A 0.007!	0.0006	A 0.14!	A 0.010!	A 0.009!	A 1.21!	56.5
Min Cal	**10.00**	**0.100**	**0.0004**	**0.0005**	**0.0002**	**0.0004**	**0.0005**	**0.0005**	**0.0001**	--
Rep	A 45.17!	<0.100	A 0.004!	A 0.008!	***0.0007***	A 0.14!	A 0.011!	A 0.008!	A 1.44!	***53.1***
Max Cal	**60.0**	**3.20**	**0.010**	**0.015**	**0.009**	**0.14**	**0.060**	**0.009**	**2.70**	--
Mean	A 45.17!	<0.070	A 0.004!	A 0.008!	**0.0007**	A 16.55!	A 0.011!	A 0.008!	A 1.44!	**36.75**
SD	***2.82***	***0.0000***	***0.001***	***0.0004***	***0.0001***	***0.0000***	***0.001***	***0.001***	***0.26***	***9.50***
RSD	***6.25***	***0.0000***	***35.75***	***5.43***	***11.17***	***0.0000***	***11.03***	***13.71***	***18.29***	***17.88***

Appendix 2.1: Results from the experiment to determine the density of top Al-Zn dross/ Portland pozzolana cement samples

Concrete design mix	Top Al-Zn Dross/ cement sample	1.2× Mass of Portland pozzolana cement Mc (g)	Mass of top Al-Zn Dross Md (g)	Dimensions of the mass of the top Al-Zn dross/ Portland pozzolana cement sample			The volume top Al-Zn dross/ Portland pozzolana cement cubes V $\times 10^{-4}$ (m^3)	Oven density of top Al-Zn dross samples Oδ $\times 10^4$ (g/m3)
				L1(cm)	L2(cm)	L3(cm)		
F	F1	324	30	6.09	6.24	6.35	2.41	146.9
	F2	324	30	6.17	6.29	6.21	2.41	146.9
	F3	324	30	6.10	6.31	6.23	2.40	147.5
G	G1	288	60	6.18	6.19	5.85	2.23	156.05
	G2	288	60	6.22	6.20	5.88	2.27	153.3
	G3	288	60	6.04	6.21	5.73	2.15	161.86
H	H1	252	90	6.35	6.11	6.00	2.33	146.78
	H2	252	90	6.36	6.11	5.13	1.99	171.86
	H3	252	90	6.17	6.15	5.28	2.00	171
I	I1	216	120	6.02	5.92	5.0	1.78	188.76
	I2	216	120	6.09	5.90	5.91	2.12	158.49
	I3	216	120	6.20	6.24	5.16	2.0	168
J	JI	180	150	6.22	6.24	5.30	2.06	160.19
	J2	180	150	6.10	6.20	5.16	1.95	169.23
	J3	180	150	6.10	6.22	4.16	1.58	208.86

Appendix 3.1: Results from the experiment to determine the porosity of the top/ cement specimens

Concrete mix design	Top Al-Zn dross/ Portland pozzolana cement sample	Mass of top Al-Zn Dross Md (g)	Weight under water W1 (g)	Dry weight W2 (g)	The volume of the top Al-Zn Dross/ Portland pozzolana Cement specimen V $\times 10^{-4}(m^3)$	Calculated porosity Vr (%)
F	F1	30	156	361	2.41	14.9
	F2	30	145	344	2.41	17.4
	F3	30	159	352	2.40	19.6
G	G1	60	159	338	2.23	19.7
	G2	60	170	355	2.27	18.5
	G3	60	166	346	2.15	16.3
H	H1	90	175	356	2.33	22.3
	H2	90	172	341	1.99	15.1
	H3	90	165	328	2.00	18.5
I	I1	120	155	297	1.78	23.6
	I2	120	165	327	2.12	21.7
	I3	120	156	304	2.0	26
J	JI	150	155	293	2.06	33
	J2	150	160	290	1.95	33.3
	J3	150	150	275	1.58	21

Appendix 4.1: Results from the experiment to determine the Coefficient of permeability

Cast specimen design mix	Top Al-Zn dross/ portlant pozzolana cement specimens	% mass of top Al-Zn dross in the sample %	Dimensions of the mass of the top Al-Zn dross/ portlant pozzolana cement specimens (mm)			Volume of water Q seeped in time t $\times 10^3$ (mm^3)	Cross-sectional area A of the top Al-Zn dross specimen $\times 10^4$ (mm^2)	Water head H (mm)	Permeability coefficient K (mm/s)
			L1	L2	L3				
F	W1	10	926	931	103	0	86.2	536	0
	W2	10	932	926	102	0	86.3	540	0
	W3	10	929	925	107	1	85.9	531	0
G	VI	20	924	926	103	231	85.6	517	0.0018
	V2	20	923	926	107	132	85.5	530	0.0010
	V3	20	915	930	108	285	85.1	546	0.0022
H	U1	30	914	927	107	2870	84.7	544	0.0222
	U2	30	929	924	103	560	85.8	522	0.0043
	U3	30	927	927	106	774	85.9	527	0.0060
I	T1	40	890	904	105	490	80.4	530	0.0040
	T2	40	902	900	107	524	81.2	537	0.0043
	T3	40	906	907	109	280	82.2	530	0.0023
J	S1	50	919	918	100	294	84.4	540	0.0022
	S2	50	921	922	102	270	84.9	535	0.0021
	S3	50	908	904	107	804	82.1	530	0.0066

Appendix 5.1: Results from the compressional strength test

Top Al-Zn dross/ cement slab	% mass of top Al-Zn dross in the sample (%)	Fracture force (KN)	Cross-sectional Area A $\times 10^4$ (mm^2)	Compressional strength Cs $\times 10^{-3}$ (N/mm^2)
W1	10	6.98	86.2	8.0974
W2	10	7.6	86.3	8.8065
W3	10	8.1	85.9	9.4296
V1	20	7.2	85.6	8.4112
V2	20	8.4	85.5	9.8246
V1	20	5.72	85.1	6.7215
U1	30	4.78	84.7	5.643
U2	30	6.14	85.8	7.1562
U3	30	7.43	85.9	8.6496

Appendix 6.1: The optimum percentage mass of top Al-Zn dross in the mix